

1 **Microglial large extracellular vesicles propagate early synaptic** 2 **dysfunction in Alzheimer's disease**

3 Martina Gabrielli,¹ Ilaria Prada,¹ Pooja Joshi,¹ Chiara Falcicchia,² Giulia D'Arrigo,¹ Grazia
4 Rutigliano,^{3,4} Elisabetta Battocchio,^{1,5} Rossella Zenatelli,⁶ Francesca Tozzi,⁷ Annalisa
5 Radeghieri,^{6,8} Ottavio Arancio,^{9,10,11} Nicola Origlia² and Claudia Verderio¹

6
7 1 CNR Institute of Neuroscience, Veduggio al Lambro, MB, 20854, Italy

8 2 CNR Institute of Neuroscience, Pisa, 56124, Italy

9 3 Institute of Life Sciences, Sant'Anna School of Advanced Studies, Pisa, 56127, Italy

10 4 CNR Institute of Clinical Physiology, Pisa, 56124, Italy

11 5 School of Medicine and Surgery, University of Milano-Bicocca, Monza, 20900, Italy

12 6 Department of Molecular and Translational Medicine, University of Brescia, Brescia, 25123,
13 Italy

14 7 Bio@SNS laboratory, Scuola Normale Superiore, Pisa, 56124, Italy

15 8 Consorzio Sistemi a Grande Interfase (CSGI), Department of Chemistry, University of
16 Florence, Sesto Fiorentino, FI, 50019, Italy

17 9 Department of Pathology and Cell Biology, Columbia University, New York, NY, 10032, USA

18 10 The Taub Institute for Research on Alzheimer's Disease and the Aging Brain, Columbia
19 University, New York, 10032, NY

20 11 Department of Medicine, Columbia University, New York, NY, 10032, USA

21

- 1 Correspondence to: Claudia Verderio
- 2 CNR Institute of Neuroscience, via Raoul Follerau 3, Veduggio al Lambro, MB, 20854, Italy
- 3 E-mail: c.verderio@in.cnr.it
- 4 Correspondence may also be addressed to: Nicola Origlia
- 5 CNR Institute of Neuroscience, via Moruzzi 1, Pisa, 56124, Italy
- 6 E-mail: origlia@in.cnr.it
- 7 **Running title:** Extracellular vesicles propagate synaptopathy
- 8

ACCEPTED MANUSCRIPT

1 Abstract

2 Synaptic dysfunction is an early mechanism in Alzheimer's disease that involves progressively
3 larger areas of the brain over time. However, how it starts and propagates is unknown.

4 Here we show that A β released by microglia in association with large extracellular vesicles (A β -
5 EVs) alters dendritic spine morphology *in vitro*, at the site of neuron interaction, and impairs
6 synaptic plasticity both *in vitro* and *in vivo* in the entorhinal cortex-dentate gyrus circuitry. 1 h
7 after A β -EV injection into the mouse entorhinal cortex, long-term potentiation (LTP) was
8 impaired in the entorhinal cortex but not in the dentate gyrus, its main target region, while 24 h
9 later it was impaired also in the dentate gyrus, revealing a spreading of LTP deficit between the
10 two regions. Similar results were obtained upon injection of EVs carrying A β naturally secreted
11 by CHO7PA2 cells, while neither A β_{42} alone nor inflammatory EVs devoid of A β were able to
12 propagate LTP impairment. Using optical tweezers combined to time-lapse imaging to study A β -
13 EV-neuron interaction, we show that A β -EVs move anterogradely at the axon surface and that
14 their motion can be blocked through annexin-V coating. Importantly, when A β -EV motility was
15 inhibited, no propagation of LTP deficit occurred along the entorhinal-hippocampal circuit,
16 implicating large EV motion at the neuron surface in the spreading of LTP impairment.

17 Our data indicate the involvement of large microglial EVs in the rise and propagation of early
18 synaptic dysfunction in Alzheimer's disease, and suggest a new mechanism controlling the
19 diffusion of large EVs and their pathogenic signals in the brain parenchyma, paving the way for
20 novel therapeutic strategies to delay the disease.

21
22 **Keywords:** microglia; extracellular vesicles; amyloid-beta; Alzheimer's disease; long-term
23 potentiation

24

1 **Abbreviations:** A β = amyloid-beta; A β ₄₂ = amyloid-beta 1-42; ACSF = artificial CSF; APP =
2 amyloid precursor protein; CHO = Chinese Hamster Ovary; CONAN = COlorimetric
3 NANoplasmonic assay; Cryo-EM = cryo electron microscopy; DG = dentate gyrus; DIV = days
4 *in vitro*; EC = entorhinal cortex; EVs = extracellular vesicles; FP = extracellular field potentials;
5 HFS = high-frequency stimulation; IL-1 β = interleukin 1 beta; INF- γ = interferon gamma; KRH
6 = Krebs-Ringer HEPES solution; LTP = long-term potentiation; mEPSCs = miniature excitatory
7 post-synaptic currents; miRNA = micro RNA; PP = perforant pathway; PrP = prion protein; PS =
8 phosphatidylserine; PTX = picrotoxin; RFP = red fluorescent protein; SAP = co-separated
9 exogenous single and aggregated proteins; TBS = theta bursts stimulation; TNF- α = tumor
10 necrosis factor alpha; TRPS = Tunable Resistive Pulse Sensing technique; TTX = tetrodotoxin.

11

1 Introduction

2 Alzheimer's disease is a progressive degenerative encephalopathy characterized by loss of
3 memory and reasoning, profound behavioral disorders and personality changes, leading to
4 dementia and death. Neuropathological hallmarks of the disease are loss of synapses and
5 neurons, extracellular amyloid-beta ($A\beta$) deposition and intraneuronal tau aggregation.¹
6 Activation of microglia, the immune cells of the brain, is an additional feature of the disease.²
7 It has been proposed that Alzheimer's pathology originates in specific areas of the brain and then
8 spreads to progressively larger regions over time, following an anatomically defined pattern of
9 connections.³⁻⁸ Extensive literature identifies synaptic dysfunction as an early mechanism
10 affected in the disease,⁹⁻¹³ which correlates with cognitive decline.^{12,14} However, how synaptic
11 dysfunction originates and propagates in the affected brain is still largely obscure, and it is now
12 one of the most compelling questions in Alzheimer's disease research.

13 $A\beta$ 1-42 ($A\beta_{42}$) has been long related to Alzheimer's disease pathogenesis as a key factor (for an
14 exhaustive review see ¹⁰). In its toxic oligomeric form,^{15,16} $A\beta_{42}$ is able to profoundly alter
15 synaptic function, typically affecting synaptic plasticity and ultimately leading to synapse
16 loss.^{9,15,17-21}

17 The circuit connecting the entorhinal cortex (EC) to the dentate gyrus (DG) of the hippocampus
18 via the perforant path (PP) represents a useful model to study synaptic dysfunction and its
19 propagation in the early disease stages. In fact, the enthorinal-hippocampal circuit plays a pivotal
20 role in various forms of memory including episodic memory,^{22,23} typically impaired in
21 Alzheimer's patients, and is one of the most vulnerable and early affected regions in the
22 disease.²⁴⁻²⁶ According to a MRI longitudinal study, the EC, followed by the hippocampal
23 formation, are the brain regions showing the first morphological alterations in Alzheimer's
24 disease, well before the clinical onset.²⁷ Significant loss of neurons occurs in EC layer II at early
25 pathological stages,²⁸ and this deficit is associated with synaptic loss in the hippocampal regions
26 receiving PP afferent input in subjects with mild cognitive impairment.²⁹ Irrespective of the
27 primary site of origin of Alzheimer's disease, studies support the hypothesis that EC is a source
28 of $A\beta$ in the mouse hippocampus: lesions of the EC or transecting the PP reduce $A\beta$
29 accumulation in the DG of transgenic APP/PS1 mice.^{30,31} Interestingly, it has been reported that

1 prevalent overexpression of mutant amyloid precursor protein (APP)/A β in the EC mediates
2 trans-synaptic propagation of A β -induced neuronal dysfunction from the EC to the hippocampus,
3 up to altering cortical network activity, and elicits Alzheimer-like behavioral deficits in mice.¹³

4 Recent advances in genetic and transcriptomic studies have pointed to microglia-related
5 pathways as central to Alzheimer's disease risk and pathogenesis.³²⁻³⁷ Neuroinflammation occurs
6 early in Alzheimer's disease,^{38,39} with microgliosis even preceding plaque formation,⁴⁰
7 suggesting an unexpected pathological role for microglia in the first stages of the disease. A few
8 mechanisms have been involved in Alzheimer's disease pathogenesis by inappropriately
9 activated microglia: excessive synaptic pruning,⁴¹ and release of synaptotoxic A β /tau in
10 association with extracellular vesicles (EVs).⁴²⁻⁴⁶

11 EVs are a heterogeneous population of membrane vesicles formed at the *plasma membrane*
12 (ectosomes/microvesicles) or in the endocytic compartment (exosomes), which contain and
13 transfer cellular components from a donor to a recipient cell.⁴⁷⁻⁴⁹ Importantly EV cargo includes
14 pathological proteins such as A β , which is stored both in EV lumen and at EV surface.^{42,43,50,51}
15 Given the difficulties in partitioning EVs into microvesicles and exosomes without cross-
16 contamination, they are now preferentially classified by size and other physical characteristics
17 (density, biochemical composition) in small (\leq 100-200 nm diameter) and large ($>$ 200 nm
18 diameter) EVs.⁵² Despite a previous study showed that microglial production of large EVs
19 carrying synaptotoxic A β species (A β -EVs) correlates with early brain damage in prodromal
20 Alzheimer's disease,⁵³ whether and how this less studied EV population contributes to initial
21 synaptic dysfunction remains elusive.

22 In this study, we sought to investigate whether large A β -EVs produced by microglia impair
23 synaptic plasticity and propagate synaptic dysfunction by moving at the axon surface. This
24 hypothesis has been suggested by our recent work indicating that large astrocyte-derived EVs
25 use neurites as routes to move extracellularly among connected neurons.⁵⁴ We show that large
26 microglial A β -EVs affect synaptic plasticity both in culture and in slices and, once injected in the
27 mouse brain, propagate synaptic dysfunction in the entorhinal-hippocampal circuit through a
28 mechanism sensitive to annexin-V, a phosphatidylserine (PS) ligand blocking EV extracellular
29 motion.

1 **Materials and Methods**

2 **Animals**

3 C57BL/6 E18-19 mouse embryos, P2 newborn and adult mice (purchased from Charles River,
4 Lecco, Italy) were employed. All experimental procedures involving animals followed the
5 guidelines defined by the European legislation (Directive 2010/63/EU), and the Italian
6 Legislation (LD no. 26/2014). The Organism Responsible for Animal Welfare (OPBA) of
7 National Research Council of Italy (CNR) Institute of Neuroscience in Milan-Pisa and the Italian
8 Ministry of Health approved the study protocols (authorizations 2D46A.N.KBG and 233/2019-
9 PR).

10 **Primary cultures**

11 Mixed glial cultures were established from postnatal day 2 (P2) C57BL/6 mice of either sex
12 (Charles River), while hippocampal neurons were established from the hippocampi of C57BL/6
13 E18-19 mouse embryos of either sex (Charles River), as previously described.⁵⁵ See
14 Supplementary Information.

15 **A β treatment**

16 Microglia primary cultures were exposed to 2 μ M human A β 1-42 (A β ₄₂, reconstituted in
17 DMSO; cat. AS-20276, AnaSpec, Eurogentec, Liège, Belgium) for 20 h, as previously
18 described.⁴²

19 **CHO7PA2 conditioned medium**

20 CHO7PA2 cells are Chinese Hamster Ovary (CHO) cell lines stably transfected with human
21 APP₇₅₁ bearing the Val717Phe mutation (7PA2 cells). Transfected cells have been kindly gifted
22 by Dr. Selkoe (Harvard Medical School, Boston, MA, USA) and maintained according to
23 Podlisny *et al.*⁵⁶. CHO7PA2 conditioned medium, containing A β species at nanomolar
24 concentrations, was collected according to Podlisny *et al.*⁵⁶. See Supplementary Information.

1 **Immunostaining of microglia-internalized A β**

2 Immunostaining of microglia-internalized A β has been performed as in ⁴², using 1:100 Isolectin
3 GS-IB4 From Griffonia simplicifolia, Alexa Fluor™ 568 Conjugate (Invitrogen # I21412,
4 Thermo Fisher Scientific, Waltham, MA, USA) on living cells and 6E10 mouse anti- β -amyloid
5 1-16 antibody (1:100; Biologend, previously Covance cat. #SIG-39300; San Diego, CA, USA)
6 after fixation. See also Supplementary Information.

7 **EV isolation**

8 Large EV-enriched samples were isolated through differential centrifugation, upon ATP
9 stimulation in a physiological solution (Krebs-Ringer's-HEPES solution, KRH) following a
10 protocol fine-tuned in the lab.⁵⁵ See also Supplementary Information.

11 **Western blotting**

12 Western Blotting was performed as in ⁵⁷, using rabbit anti-Alix (1:500; Covalab, Villeurbanne,
13 France), mouse anti-Flotillin (1:1000, BD Biosciences, CA, USA), rabbit anti-Annexin A2
14 (1:5000, Abcam, UK), rabbit anti-GAPDH (1:1000, #247002, Synaptic Systems, Gottingen,
15 Germany), mouse anti-GS28 (1:1000; BD Biosciences, Franklin Lakes, NJ, USA), rabbit anti-
16 TOM20 (1:500; Santa Cruz Biotechnology, CA, USA), and mouse anti-A β 6E10 (1:1000;
17 Biologend, previously Covance cat. #SIG-39300). See also Supplementary Information.

18 **Colorimetric NANoplasmonic (CONAN) assay**

19 EV preparations from A β ₄₂-treated-microglia and control cells were characterized for purity from
20 contaminants, referred to as co-separated soluble exogenous single and aggregated proteins
21 (SAPs), with the COlorimetric NANoplasmonic (CONAN) assay, following the open-access
22 protocol by Zendrini *et al.*⁵⁸. See Supplementary Information.

23 **EV characterization by TRPS**

24 Tunable Resistive Pulse Sensing (TRPS) technique, by Izon qNano instrument (Izon,
25 Christchurch, New Zealand), was used to measure the size distribution and concentration of 10

1 000xg (large) A β -EV fractions, as well as their surface charge. See also Supplementary
2 Information.

3 **A β quantification in EVs**

4 Quantitative determination of A β ₄₂ in EVs was performed using Human A β 42 ELISA Kit
5 (Invitrogen cat. KHB3441, Thermo Fisher Scientific). 10 000xg (large) A β -EV pellets were
6 resuspended in Standard Diluent Buffer from the kit, supplemented with 1:100 Halt Protease
7 Inhibitor (Thermo Fisher Scientific) and 1 mM phenylmethylsulfonyl fluoride (PMSF, Merck,
8 Darmstadt, Germany). Lysed EV samples were solubilized with 0.57% Triton X-100 (Merck)
9 followed by 20 s vortexing (as described in ^{59,60}). The assay was performed according to the
10 manufacturer's protocol. Halt Protease Inhibitor, PMSF and Triton X-100 were added to A β
11 Standards at the same concentration as in the samples. Absorbance was detected at 450 nm using
12 a Wallac 1420 Multilabel Counter - Victor2 (Perkin-Elmer, Waltham, MA, USA).

13 **Cryo-EM of EVs**

14 Freshly prepared 10 000xg (large) A β -EV pellets resuspended in saline were plunge frozen in
15 liquid ethane using a Vitrobot Mk IV (Thermo Fisher Scientific). Images of the vitrified
16 specimen were acquired using a Talos Arctica transmission electron microscope (Thermo Fisher
17 Scientific). See also Supplementary Information.

18 **Annexin-V treatment**

19 10 000xg (large) A β -EV pellet was resuspended in 300 μ l Krebs-Ringer's HEPES solution
20 (KRH) (in mM, 125 NaCl, 5 KCl, 1.2 MgSO₄, 1.2 KH₂PO₄, 2 CaCl₂, 6 D-glucose, 25
21 HEPES/NaOH, pH 7.4) and annexin-V (A7810, Merck) was added at an active concentration of
22 8.4 μ g/ml for 30 min on a low-speed wheel at room temperature. Subsequently, 1 ml KRH was
23 added to the sample to dilute the molecule and EVs were re-pelleted at 10 000 \times g for 30 min at
24 4°C.

1 **Optical tweezer experiments**

2 Optical trapping and manipulation of EVs was performed following the approach previously
3 described.^{54,61} In order to distinguish dendrites from axons, 12×10^4 neurons on 24 mm glass
4 coverslips were transfected with RFP (red fluorescent protein) using Lipofectamine 2000
5 (Invitrogen, Thermo Fisher Scientific). Before recording, neurons were washed to remove EVs
6 constitutively released by neurons and large-EVs (10 000xg pellet) produced by $\sim 1 \times 10^5$
7 microglia were added to neurons and maintained in 500 μ l of phenol red-free neuronal medium
8 in a 5% CO₂ and temperature-controlled recording chamber at 37°C. See also Supplementary
9 Information.

10 **Dendritic spine analysis**

11 14-17 DIV 12×10^4 neurons (on 24 mm glass coverslips) were imaged with a 63 \times objective using
12 an Axiovert 200 M equipped with spinning disk microscope prior and 2, 10, 20, 30, 40 min after
13 placing single EV on an RFP-positive dendrite through optical manipulation. Acquisition
14 software was Velocity 6.3.0 (Perkin Elmer). Analysis was performed only when the EV adhered
15 to the dendrite. Focal planes were stacked together in a max intensity projection, and RFP-
16 positive spines were analyzed in the vicinity of EV contact site (<7 μ m from the contact point),
17 far from the contact site (>60 μ m from the contact point) or along the entire dendrite. Spine
18 morphology was analyzed using ImageJ software (<http://imagej.nih.gov/ij/>). Spines were
19 classified in categories (mushroom, thin, stubby) based on morphological parameters: spine head
20 diameter (H), spine length (L) and spine neck width (N), according to NeuronStudio software
21 criteria, as in⁵⁷.

22 **Tracking of single EV on neurons**

23 After placing the EV on 13-17 DIV neurons, cells were live imaged using a digital camera (High
24 Sensitivity USB 3.0 CMOS Camera 1280 \times 1024 Global Shutter Monochrome Sensor, Thorlabs,
25 Newton, NJ, USA) at a frame rate of 2 Hz for 40 min. Videos were saved as *.AVI file for
26 offline analysis. EV position was determined for each video frame (considering two frames every
27 5 seconds) using a custom MATLAB code (it.mathworks.com). To evaluate EV displacement on
28 the neuron process, 2 distances were calculated: the length of the path traveled by the EV in the

1 first 10 minutes after contact (pathlength) and the max distance covered by the EV from the
2 contact point in both direction in the first 10 minutes after contact (sum of distances reached by
3 the EV in both directions). Mean velocity and distances were extracted from EV coordinates
4 using a custom R code (www.r-project.org) that exploits the Pythagorean Theorem to reconstruct
5 the EV path point-to-point. We classified as “static EVs” i) the EVs with net displacement < of
6 the EV diameter and ii) EVs showing only random (Brownian) motion.

7 **Subcellular localization of large mCLING-labelled EVs**

8 Labelling of EVs with mCLING was performed according to ⁶². Briefly, EVs in the 10 000xg
9 pellet were resuspended in 500 µl of sterile and 0.1 µm filtered PBS and incubated with 400 nM
10 mCLING-ATTO 647N-labeled (Synaptic System, Goettingen, Germany) in a black tube on ice
11 for 5 minutes. The reaction was quenched by adding 500 µl of 1% BSA in PBS. Then, EVs were
12 diluted in 10 ml of PBS, re-pelleted at 10 000xg to eliminate the dye excess, resuspended in
13 neuronal medium and added to membrane-targeted GFP-transfected hippocampal neurons for 1 h
14 before fixing the cells with 4% paraformaldehyde–4% sucrose (w/v) for 8 minutes. Coverslips
15 were then mounted on a microscope slide and Z-stacks were acquired with a Zeiss LSM800
16 confocal microscopy (Oberkochen, Germany). Analysis of EV localization on axons was
17 performed on ImarisViewer 9.7.2.

18 **Immunofluorescence analysis of juxtaposed pre-/post-synaptic** 19 **puncta**

20 8×10^4 neurons on 24 mm coverslips were incubated with 0.6×10^8 /ml EVs for 3 h, then fixed with
21 4% paraformaldehyde–4% sucrose (w/v) and stained with guinea-pig anti-Bassoon (Synaptic
22 Systems, Cat# 141 004, RRID:AB_2290619) and rabbit anti-Shank-2 (Synaptic Systems Cat#
23 162 202, RRID:AB_2619860) primary antibodies, followed by Alexa-555 and Alexa-488
24 secondary antibodies (1:200, Alexa, Invitrogen). Analysis was performed according to ⁵⁷. See
25 Supplementary Information.

1 **Electrophysiology on cell culture**

2 7×10^4 mature hippocampal neurons in culture on 15 mm coverslips were incubated with 2×10^7
3 ctrl-EVs or A β -EVs in 330 μ l, or vehicle, for 1 h. To record miniature excitatory post-synaptic
4 currents (mEPSCs), the voltage-gated Na⁺-channel blocker tetrodotoxin (TTX, 0.5 μ M, Alomone
5 Labs, Jerusalem, Israel) and the GABA-A receptor antagonist picrotoxin (PTX, 100 μ M, Merck)
6 were added to the bath solution, along with strychnine (1 μ M, Merck), used to avoid glycine
7 receptor activation. In order to investigate synaptic plasticity, after 12 min baseline recording in
8 standard bath solution, Mg²⁺-free bath solution was perfused for 1 min before applying the same
9 solution containing glycine (Gly, 200 μ M, Merck) for 3 min. Subsequently, perfusion was
10 resumed with standard Mg²⁺-containing bath solution and recording will continue for 40 min.
11 Potentiation magnitude was measured as the average response between the 28th and the 40th min
12 after glycine. See also Supplementary Information.

13 **Stereotaxic EC injection**

14 For stereotaxic injections, 2-3 months C57BL/6 mice (male and female in equal number) were
15 deeply anesthetized using urethane (Merck, 20% solution, 0.1 ml/100 g of body weight) via
16 intraperitoneal injection. After tail pinch reflex disappearance, mice were positioned in a
17 stereotaxic apparatus. The scalp was shaved and a midline incision was made. Two holes were
18 drilled bilaterally at stereotaxic coordinates targeting the LEC (AP -3.8 mm, ML \pm 4.0 mm from
19 Bregma, measured on the skull surface). An injecting needle was then inserted through the holes
20 and 1 μ l of EVs ($0.25 \times 10^8/\mu$ l or $0.11 \times 10^8/\mu$ l in artificial CSF (ACSF)), soluble oligomeric A β_{42}
21 alone (100 nM in ACSF; prepared as previously described⁶³) or ACSF alone (vehicle) was
22 slowly injected 4 mm below the dura. ACSF composition was the following (in mM): 119 NaCl,
23 2.5 KCl, 2 CaCl₂, 1.2 MgSO₄, 1 NaH₂PO₄, 6.2 NaHCO₃, 10 glucose, 10 HEPES. The pipette
24 remained in place at the injection site for 2 minutes before slow removal. Then, the scalp was
25 sutured and the mouse was brought back to its cage for recovery.⁶⁴

26 **Slice preparation**

27 1 h or 24 h after EC injection, animals were sacrificed and EC/hippocampal slices were cut as
28 described.⁶⁵ See Supplementary Information.

1 **Electrophysiology in slices**

2 Extracellular field potentials (FPs) and whole cell patch-clamp recordings were performed as
3 previously described.^{65,66} See Supplementary Information.

4 **Statistical analysis**

5 Statistical analysis was performed using SigmaStat 3.5 for Windows (Systat Software Inc., San
6 Jose, CA, USA). Normality test was performed for all data sets and the proper statistical test was
7 selected accordingly. Two-tailed statistical tests have been performed if not otherwise stated.
8 Data are shown as mean \pm SEM. Optical tweezer's data of adhering/moving EVs are expressed
9 as raw percentage on total tested EVs (i.e. total number of EVs placed on axons, no average) and
10 analyzed by chi-square test. Chi-square is the appropriate statistical test to compare raw
11 percentages, to determine if there is a significant difference in the distribution of a group among
12 different categories beyond what can be attributed to random sampling variation (e.g. for EVs,
13 categories were: adhered/didn't adhere, moved/didn't move). Differences were considered
14 significant when $p < 0.05$ and indicated by asterixis: $p < 0.05$, *; $p < 0.01$, **; $p < 0.001$, ***. n
15 indicates the number of measurements taken from distinct samples. *A priori* sample size
16 calculations have been performed using G*Power 3 software (Heinrich Heine Universität,
17 Düsseldorf, Germany). See also Supplementary Information.

18 **Data availability statement**

19 The data that support the findings of this study are available from the corresponding authors
20 upon reasonable request. The R custom code used for EV analysis is available at
21 <https://doi.org/10.6084/m9.figshare.12808211.v1>.

22 **Results**

23 **Isolation of large A β -EV enriched fraction and characterization**

24 Primary murine microglia were exposed to 2 μ M exogenous beta-amyloid 1-42 (A β ₄₂) for 20 h to
25 allow A β ₄₂ internalization and then were activated with 1 mM adenosine triphosphate (ATP) to

1 stimulate the release of EVs carrying A β forms (A β -EVs), as previously characterized.^{42,43}
2 Samples enriched in large A β -EVs or large ctrl-EVs, released by microglia not exposed to A β ₄₂,
3 were isolated according to MISEV2018 guidelines,⁵² by differential centrifugation at 10 000xg
4 after pre-clearing of cell supernatant from cells and debris at 300xg, as previously established in
5 our laboratory.^{42,55}

6 Western blotting analysis indicated that large microglial EVs released upon short (up to 1 h)
7 stimulation with ATP and isolated by differential centrifugation are positive for the EV markers
8 flotillin 1, alix and annexin-A2, a typical marker of large EVs, and almost unstained for
9 intracellular organelle markers (GS28 and TOM20, for Golgi and mitochondria respectively) or
10 the cytosolic marker GAPDH (Fig. 1A and Supplementary Fig. 1 for normalization to total
11 proteins). As expected, A β -EVs contained A β , as indicated by positive staining for anti-A β 6E10
12 antibody, with A β being highly enriched in EVs compared to donor cells (about 10-fold change,
13 Fig. 1A). The purity of EV preparations was corroborated by analysis with the Colorimetric
14 NANoplasmonic (CONAN) assay, which consists of a solution of gold nanoparticles (AuNPs)
15 into which EVs are added. The solution turns blue if the EV preparation is pure, whereas it stays
16 red if protein contaminants are present. Quantification of the color change provides an
17 aggregation index (AI), which is an index of purity. Results reported in Fig. 1B show that both
18 the EV preparations from A β ₄₂-treated-microglia and control cells reach AI lower than 20%,
19 indicating that in both samples contaminants are below 0.05 $\mu\text{g}/\mu\text{L}$ ⁵⁸ (Fig. 1B).

20 Large A β -EV enriched fractions were highly heterogeneous in size, ranging from 92 nm to 1.7
21 μm as indicated by tunable resistive pulse sensing (TRPS) analysis (Fig. 1C). Large A β -EVs had
22 a mean size of 315.00 ± 5.68 nm, with a mode of 140.00 nm. According to this method, the
23 percentage of large EVs above 200 nm was ~59%. A β -EV production was rated to $\sim 0.5 \times 10^8$ EVs
24 ($4.66 \times 10^7 \pm 1.55 \times 10^7$; n=4) from 1 million cells in 1 h, similar to microglia not exposed to A β .⁵⁷

25 Following EV solubilization with 0.57% Triton X-100^{59,60} and ELISA A β ₄₂ measurement, we
26 found that 0.5×10^8 large A β -EVs isolated at 10 000xg contain ~370 pg of A β ₄₂. Similar amount
27 of A β was detected in small A β -EVs pelleted at 100 000xg (~330 pg). Half of the amount of
28 A β ₄₂ was detected in intact A β -EVs, not treated with the detergent, in the large EVs enriched
29 fraction (Fig. 1E), suggesting that A β is located both in the lumen and at the outer surface of A β -
30 EVs, as previously described.^{42,43,50,51} Consistent with the presence of A β species enriched in

1 negatively charged residues⁶⁷ at the EV surface, Z-potential analysis revealed a significant
2 negative shift in the surface charge compared to ctrl-EVs (produced by microglia not exposed to
3 A β) (-22.57 mV A β -EVs vs. -10.75 mV ctrl-EVs) (Fig. 1D). Interestingly, A β ₄₂ content in large
4 EVs-enriched fraction raised significantly when microglia were exposed to Bafilomycin A1 (25
5 nM) to block intracellular degradative pathways (Fig. 1F), indicating a role for EVs in A β
6 disposal. EV production was not affected by Bafilomycin treatment (Fig. 1G). Large A β -EVs
7 enriched fraction was further characterized by cryo-electron microscopy, which confirmed large
8 heterogeneity in vesicle size and morphology (Fig. 1H). Most A β -EVs were uni-lamellar, round
9 and with smooth surface but we observed examples of multi-lamellar and tubular vesicles (Fig.
10 1H, arrows and white arrowheads, respectively) or with rough surface (Fig. 1H, black
11 arrowheads).

12 Collectively these findings showed that large EVs are highly enriched in A β species generated
13 from A β ₄₂ internalized in microglia and confirmed that part of A β ₄₂ is exposed on the EV
14 surface. Because large A β -EVs can be monitored by bright field microscopy, in this study we
15 focused on this population of less studied EVs to analyze their impact on synaptic morphology
16 and function.

17 **Large A β -EVs affect dendritic spine morphology and synaptic** 18 **plasticity *in vitro***

19 Dendritic spines are post-synaptic elements of excitatory neurons, whose size is correlated with
20 synapse strength, hinting at a possible structural mechanism at the basis of synaptic plasticity.⁶⁸
21 To explore the possible contribution of A β -EVs to synaptic dysfunction, we first characterized
22 the action of large A β -EVs on dendritic spine density and morphology. This investigation was
23 performed on cultured hippocampal neurons using optical tweezers, an innovative technique that
24 allows to gently placing single EV on the cell surface,⁶¹ mimicking the random attachment of
25 EVs to cultured neurons.⁵⁵

26 Neurons were transfected with cytoplasmic RFP to delineate the spine shape and time-lapse
27 imaged by spinning disk microscopy prior and 2, 10, 20, 30, 40 min after the contact of large A β -
28 EVs or ctrl-EVs with secondary dendrites (Fig. 2A). Briefly, confocal images of RFP positive
29 dendrites were first acquired. Then, in bright-field, a small amount of large EVs ($\sim 0.5 \times 10^7$), was

1 loaded into the medium and single large EV was trapped and finely placed onto the selected
2 dendrite by optical manipulation. EVs >200 nm, above the resolution limit, were more easily
3 visualized in bright-field and manipulated by the laser trap. After 30 seconds, the laser tweezers
4 were switched off and EV adhesion to the cell surface monitored. Only when EVs adhered to
5 dendrites, time-lapse confocal images were acquired (16/26 A β -EVs, 6/9 ctrl-EVs, n=13
6 experiments). Confocal analysis showed that A β -EVs or ctrl-EVs induced a significant increase
7 in the density of dendritic spines around the contact site (<7 μ m from the contact point) from 2
8 min after adhesion (Fig. 2B-C). The maximal effect was observed 30-40 minutes after contact
9 (spine density increase: 146.33 \pm 9.29 % ctrl-EVs; 133.20 \pm 13.98 % A β -EVs) (Fig. 2B-C). Almost
10 no impact of EVs (A β -EVs nor ctrl-EVs) was observed far from the contact site (>60 μ m), where
11 the spine density remained unchanged, at any time point (Fig. 2B,D), indicating that EVs act
12 locally.

13 When we classified dendritic protrusions in mature and immature, based on morphological
14 parameters (spine length, head diameter, neck width), we found that A β -EVs significantly
15 increase the number of immature (thin) protrusions at the contact site (Fig. 2B,E), while ctrl-EVs
16 enhanced the number of mature (mushroom, stubby) spines (Fig. 2B,G). No alterations in spine
17 shape were observed far from the contact site (>60 μ m) (Fig. 2B,F,H). Consistent with a local
18 EV action, changes in dendritic spine density and morphology were less pronounced when
19 measured along the entire length (~80 μ m) of the dendrite in contact with A β -EVs or ctrl-EVs,
20 40 min after adhesion (Supplementary Fig. 2A). Interestingly, A β -EV induced spine thinning
21 involved both newly generated (Supplementary Fig. 2B) and pre-existing protrusions
22 (Supplementary Fig. 2C).

23 By decreasing the spine size, A β -EVs might affect synapse stability upon longer exposure. To
24 assess this hypothesis, we next exposed hippocampal neurons to large A β -EVs (0.6×10^8 EVs/ml,
25 i.e. 49 pM surface A β_{42}), ctrl-EVs (0.6×10^8 EVs/ml) or vehicle for 3 h in bulk. Cultures were
26 then fixed and stained for the pre-synaptic active zone protein Bassoon and the post-synaptic
27 marker Shank-2. Analysis of Bassoon and Shank-2 double positive puncta showed a significant
28 decrease in juxtaposed pre- and post-synaptic terminals in A β -EV-treated compared to vehicle-
29 treated or ctrl-EV-treated neurons (Fig. 2I-J), revealing that A β -EVs impair synaptic stability on
30 a longer time scale. Conversely, ctrl-EVs did not increase the number of juxtaposed pre- and
31 post-synaptic terminals, suggesting that dendritic spines formed shortly after ctrl-EV-neuron

1 contact do not assemble with presynaptic boutons to make stable synaptic terminals in the
2 long/medium term.

3 Next, we asked whether dendritic spine alterations were associated with changes in synaptic
4 plasticity. Neurons were exposed to A β -EVs, ctrl-EVs or vehicle for 1 h (0.6×10^8 EVs/ml), as
5 described above. After treatment, EVs were washed out and miniature excitatory post-synaptic
6 currents (mEPSCs), corresponding to the spontaneous and random release of neurotransmitter
7 from the pre-synaptic terminal, were measured through single cell whole-cell patch clamp
8 recordings. When synaptic plasticity was evoked using a protocol that chemically induces
9 potentiation through a brief application of glycine (3 min, 200 μ M, in Mg²⁺-free solution),⁶⁹ we
10 found that neurons treated with A β -EVs lost their capability of undergoing a long-lasting
11 increase in mEPSC frequency compared to vehicle and ctrl-EV treated neurons (Fig. 2K-L).
12 Accordingly, immunofluorescence analysis of puncta positive for the post-synaptic marker PSD-
13 95 and the pre-synaptic marker VGlut-1 before and after chemical LTP⁷⁰ revealed that the area
14 of PSD-95 positive and VGlut-1/PSD-95 double positive puncta does not increase in A β -EVs-
15 treated neurons after plasticity induction, as opposed to vehicle-treated neurons (Supplementary
16 Fig. 3). Collectively, these data indicate that A β -EVs selectively affect synaptic plasticity in
17 cultured neurons.

18 **Large A β -EVs move along the axons of cultured neurons**

19 Our recent work shows that a fraction of large EVs derived from astrocytes moves at the surface
20 of cultured neurons exploring actin protrusions and use neurites as routes to pass between
21 connected cells.⁵⁴ Based on this evidence, we first explored whether EVs of microglial origin
22 may similarly move at the neuron surface. Through optical tweezers, we gently placed single
23 large EV on cell bodies and neurites of developing hippocampal neurons, cultured from 2 to 12
24 days *in vitro* (DIV), and examined EV-neuron interaction in bright field through live
25 microscopy. While a low percentage of microglial EVs moved on the neuron cell bodies (12.5%,
26 n=2/16), about 53% of EVs displayed extracellular motion along neurites (n=19/36), proving that
27 also large microglial EVs can use neurites to move into the extracellular space. Next, we
28 monitored the dynamics of large A β -EVs or ctrl-EVs at the axon surface of fully differentiated
29 neurons (13-17 DIV) for up to 40 min (Fig. 3A). Axons were distinguished from dendrites by

1 their smaller size and the absence of spines on RFP transfected neurons. A similar percentage of
2 large A β -EVs adhered to the axonal surface compared to ctrl-EVs (48% vs. 44%; Fig. 3E), ruling
3 out a major involvement of A β in the establishment of EV-neuron contact. After adhesion, about
4 85% of A β -EVs displayed net movement from the contact site, surfing on the axon plasma
5 membrane (Fig. 3B-C,F, Supplementary Movie), while only few A β -EVs (15%) were virtually
6 immobile (EV displacement < EV diameter) or displayed only random Brownian motion (being
7 connected to the axon by a tether) and were considered static (Fig. 3D,F). Notably, A β -EVs were
8 more prone to motility compared to ctrl-EVs, as almost twice the A β -EVs were able to move at
9 the axon surface (85% vs. 45%; Fig. 3F). Analysis of EV motion by a custom MATLAB code
10 revealed higher average speed for A β -EVs compared to ctrl-EVs (116.56 ± 20.31 nm/s vs.
11 48.20 ± 21.01 nm/s, Fig. 3G), longer pathlength (78.98 ± 14.07 μ m/10 min vs. 42.72 ± 17.19 μ m/10
12 min, Fig. 3H) and run distance from the contact point (7.55 ± 1.51 μ m/10 min vs. 4.37 ± 1.65
13 μ m/10 min, Fig. 3I). In addition, visualization of EV trajectories revealed that most A β -EVs
14 (~67%) moved in an anterograde (towards the periphery) rather than retrograde (towards the cell
15 body) direction along the axons (number of EVs=10/15, 11 experiments) (Fig. 3J), while most
16 ctrl-EVs exhibited retrograde motion (~60%, number of EVs=9/15, 7 experiments) (Fig. 3J).
17 Next, we asked what percentage of large A β -EVs could be internalized inside axons instead of
18 moving anterogradely. We labelled EVs with the fluorescent dye mCLING and analyzed by
19 confocal microscopy the localization of mCLING- labelled EVs 1 h after in bulk addition to
20 neurons transfected with membrane-targeted GFP. Confocal analysis revealed that the vast
21 majority of large A β -EVs, but also ctrl-EVs, remained outside the axons (97% A β -EVs, $n=101$
22 EVs; 97% ctrl-EVs, $n=39$ EVs; Supplementary Fig. 4), in agreement with our previous
23 observation that large EV size is a key factor retaining EVs at the neuron surface.⁵⁴ Altogether,
24 these data indicate that A β -EVs move extracellularly along axonal projections, with a prevalent
25 anterograde direction, supporting the hypothesis that they may propagate A β -mediated synaptic
26 alterations among synaptically connected neurons.

27 Notably, A β -EVs motion was significantly decreased when large EVs were pre-treated with
28 annexin-V (8.4 μ g/ml, 30 min), a molecule commonly used to inhibit signaling of large EVs to
29 receiving cells.⁷¹ Annexin V cloaks phosphatidylserine (PS) residues, externalized on the surface
30 of large EVs,⁵⁹ and alters EV-cell interaction.⁶¹ A β -EVs coated with annexin V (coated-A β -EVs)
31 adhered more efficiently to neurons (from 48% to 73% of adhesion; Fig. 3K), remained outside

1 the axons, as indicated by analysis of mCLING- coated-A β -EVs localization in GFP-expressing
2 neurons, (coated-A β -EVs outside neurons 97%, $n=63$ EVs), and moved less along the axons of
3 cultured neurons (from 85% to 44% of motion; Fig. 3L). The speed of coated A β -EVs still
4 moving at the neuron surface was not significantly affected (73.01 ± 15.66 nm/s for c- A β -EVs
5 compared to 116.56 ± 20.31 nm/s for A β -EVs) (Fig. 3M).

6 **Large A β -EVs propagate LTP impairment in the entorhinal-** 7 **hippocampal circuit**

8 Encouraged by the finding that large A β -EVs impair synaptic plasticity and move along the
9 axons of cultured neurons, we next examined whether A β -EVs may induce and spread synaptic
10 dysfunction in the adult mouse brain. First, we extrapolated findings on synaptic plasticity from
11 cell cultures to long-term potentiation (LTP), a form of synaptic plasticity thought to underlie
12 learning and memory,⁷² in the slice preparations, which have an intact neuronal circuitry. In
13 particular, we investigated whether large A β -EVs are able to impair LTP in mouse entorhinal
14 cortex (EC) slices, a crucial site for memory formation, particularly vulnerable in Alzheimer's
15 disease.^{13,26,73} Horizontal sections of entorhinal slices were treated with 1×10^8 A β -EVs/ml (equal
16 to 82 pM surface A β_{42}), ctrl-EVs (1×10^8 EVs/ml), or vehicle for 1 h. LTP was induced by high-
17 frequency stimulation (HFS; 3 trains of 100 pulses at 100 Hz, at 10 s intervals) of EC superficial
18 layer II⁶⁴⁻⁶⁶ and field potentials (FPs) were recorded from the same layer. The study of basal
19 synaptic transmission, measured through analysis of the input/output relationship, did not reveal
20 any difference between slices treated with A β -EVs, ctrl-EVs or vehicle (Fig. 4A). LTP was
21 reliably elicited in slices incubated with ctrl-EVs (Fig. 4B). The mean LTP was 131 ± 4 (SEM)
22 % of baseline amplitude 40 min after HFS, similar to vehicle treated slices. By contrast, LTP was
23 not elicited in A β -EV treated EC slices (Fig. 4B). Note that the concentration of EV surface A β_{42}
24 estimated by ELISA (82 pM) is considerably lower than that of oligomeric A β_{42} alone which
25 impairs LTP in EC slices (200 nM in our papers)^{65,66}. Thus, EVs are capable of enhancing the
26 synaptotoxic effect of A β on EC intrinsic circuitry.

27 Subsequently, we examined whether large A β -EVs may spread synaptic dysfunction in the
28 entorhinal-hippocampal circuit. Using EC-hippocampal slices,⁶⁵ we measured LTP both in the
29 EC and in its main target region, the ipsilateral dentate gyrus (DG), 1 h and 24 h after stereotaxic

1 injection of A β -EVs or ctrl-EVs (0.25×10^8 EVs, from the large EV-enriched fraction, diluted in 1
2 μl ; 20 nM A β_{42}) in the EC of adult mice (Fig. 4C). Indeed, considering the speed at which A β -
3 EVs move *in vitro* (116.56 nm/s equal to 419.62 $\mu\text{m}/\text{h}$), we reasoned that 24 h was enough time
4 in order to reach the DG moving along the perforant pathway (PP), which is 1.5-3 mm in
5 length.⁷⁴ The accuracy of the injection site was checked by injecting PKH26 Red Fluorescent
6 Dye (Merck) in the mouse brain using the same coordinates as for EVs injections (AP -3.8 mm,
7 ML ± 4.0 mm from Bregma, measured on the skull surface) (Supplementary Fig. 5).

8 Extracellular recordings from the EC superficial layer II revealed a block of LTP 1 h after A β -
9 EV injection, whereas a stable LTP was recorded in the contralateral EC injected with ctrl-EVs
10 (Fig. 4D). Extracellular recordings at the synapse between the PP and the DG (PP-DG) showed
11 normal LTP 1 h after A β -EV injection following a theta burst simulation (TBS, 10 bursts of 5
12 pulses at 100 Hz with 250 ms between bursts, as described in⁶⁴) (Fig. 4E). However, 24 h later,
13 LTP was blocked not only in the EC (Fig. 4D) but also at PP-DG synapse (Fig. 4E), indicating
14 propagation of LTP impairment between the two connected regions. Similar results have been
15 obtained injecting \sim half-dose of A β -EVs (0.11×10^8 in $1 \mu\text{l}$; 9 nM A β_{42}) (Supplementary Fig. 6).
16 On the contrary, when we unilaterally injected soluble oligomeric A β_{42} ($1 \mu\text{l}$; 100 nM) in the EC,
17 LTP was inhibited at this site 1 h after the injection but never in the DG (neither 1 h nor 24 h
18 after injection in the EC) (Fig. 4F-G). This indicates that A β_{42} alone is not able to propagate
19 among connected regions and requires EVs as vehicle for the transfer. In addition, LTP was
20 completely restored in the EC 24 h after oligomeric A β_{42} injection (Fig. 4F), revealing a short-
21 lasting action of free oligomeric A β_{42} , not associated to EVs. Collectively these findings indicate
22 that, while oligomeric A β_{42} alone transiently impairs LTP in the EC, EV-associated A β causes a
23 persistent LTP impairment that propagates along the EC-hippocampal circuit.

24 Next, we aimed at clarifying whether the effect of large A β -EVs was dependent on A β cargo or
25 other EV component(s) (protein, lipids, and miRNAs) sorted in the EVs by A β -treated microglia.
26 To this end, microglia were activated with a classical inflammatory stimulus (a cytokine cocktail:
27 50 ng/ml IL-1 β , 20 ng/ml TNF- α , 20 ng/ml INF- γ for 24 h, as in⁷⁵, which elicits some of A β -
28 induced traits in microglia and EVs (i-EVs) thereof, i.e. similar expression of a set of
29 inflammatory cytokines and miRNAs)⁵⁷. Once injected into the EC, i-EVs (0.25×10^8 large EVs
30 diluted in $1 \mu\text{l}$, same as A β -EVs) were able to impair LTP in the EC either 1 h after the injection

1 or 24 h after (Fig. 4H), similarly to A β -EVs. However, i-EVs never blocked LTP in the DG (Fig.
2 4I), revealing that only EVs carrying A β propagate LTP defects along the EC-hippocampal
3 connection.

4 **Large A β -EVs mainly act on the post-synaptic compartment of the** 5 **synapse**

6 To characterize the molecular mechanisms underlying A β -EV action on the EC-hippocampal
7 circuit, we performed single cell whole-cell patch clamp recordings on pyramidal cells of EC
8 superficial layer II and their main target cells, the granular cells of the DG, 1 h and 24 h after
9 large A β -EV injection in the EC of adult mice (0.25×10^8 EVs/1 μ l; 20 nM A β_{42}) (Fig. 5A). The
10 contralateral hemisphere was injected with vehicle. We analyzed mEPSCs, generally accepted as
11 the post-synaptic response to the spontaneous release of a single quantum of neurotransmitter. In
12 fact, a variation in their frequency is usually related to a change in probability of quantal
13 transmission from the pre-synaptic terminal, whereas a modification in their amplitude is
14 associated with post-synaptic changes. This analysis revealed that A β -EVs induce a significant
15 decrease in mEPSC amplitude, with no alteration in their frequency, in pyramidal cells of the EC
16 1 h after the injection, compared to the cells in the vehicle-injected hemisphere (Fig. 5B-C),
17 mimicking synthetic A β_{42} effect.⁶⁵ No alteration in mEPSC frequency or amplitude was detected
18 1h after ctrl-EV (0.25×10^8 EVs/1 μ l) EC injection (frequency 1.96 ± 0.60 Hz, Mann-Whitney
19 Rank Sum Test, $p=0.841$ vs.vehicle; amplitude 9.53 ± 0.81 pA, t-test, $p=0.781$ vs.vehicle; $n=9$, 3
20 mice). Interestingly, the same decrease in mEPSC amplitude was found in granular cells of the
21 DG 24 h after A β -EV injection (Fig. 5D-E). Beside confirming that large A β -EVs propagate
22 synaptic dysfunction along the PP, these data revealed that A β -EVs resemble synthetic A β_{42}
23 action, mostly acting at the post-synaptic site of the synapse.

24 **Large EVs released by microglia exposed to naturally secreted A β** 25 **impair LTP**

26 Data described above and our previous evidence indicate that microglia exposed to micromolar
27 concentration of synthetic A β_{42} (mainly in an aggregated form, mimicking extracellular A β
28 plaques) generate soluble forms of A β_{42} , A β_{40} and other truncated peptides,⁴² that once sorted

1 into large EVs cause and propagate synaptic dysfunction. As at early stages of Alzheimer's
2 disease microglia is exposed to low concentration of oligomeric A β form, we found important to
3 verify whether microglia exposed to nanomolar concentrations of native A β forms may also
4 release A β -storing EVs, which induce and propagate synaptic dysfunction. To this aim, we
5 incubated for 20 h primary microglia with medium conditioned by CHO7PA2 cells, Chinese
6 hamster ovary cells which stably express the human amyloid precursor protein (APP) bearing
7 Val717Phe mutation⁵⁶ and release oligomeric A β ²⁰ at nanomolar concentration.⁵⁶
8 Immunostaining with anti-A β antibody (6E10) showed that A β produced by CHO7PA2 was
9 internalized by microglia (Fig. 6A), albeit in smaller quantity compared to the synthetic
10 peptide.⁴² When EVs produced by microglia exposed to CHO7PA2-secreted A β (CHO-EVs)
11 were injected in the mouse EC (0.25×10^8 EVs/ μ l) and LTP was recorded in EC and PP-DG, we
12 observed impaired LTP in the EC 1 h after the injection (Fig. 6B) and at PP-DG synapses 24 h
13 later (Fig. 6C), replicating results obtained with EVs produced by microglia exposed to synthetic
14 A β ₄₂. Thus, large EVs released by microglia exposed to naturally secreted A β also cause and
15 propagate LTP deficit in the entorhinal-hippocampal circuit.

16 **Inhibition of large A β -EV extracellular motion prevents** 17 **propagation of synaptic deficits *in vivo***

18 We finally asked whether reducing EV motility along axonal projections may inhibit the
19 propagation of synaptic defects. To this end, we injected A β -EVs coated with annexin-V (c-A β -
20 EVs, 0.11×10^8 in 1 μ l, 9 nM A β ; annexin-V, 8.4 μ g/ml, 30 min), which move less *in vitro* along
21 axons (Fig. 3L), in the EC of mice. c-A β -EVs induced LTP deficit in the EC 1 h after the
22 injection (Fig. 7A), whereas LTP was still present in the DG 24 h after injection (Fig. 7B),
23 indicating that c-A β -EVs were not able to propagate synaptic defects. These data provide the
24 first evidence for the involvement of large EV extracellular motion in progression of synaptic
25 dysfunction in Alzheimer's disease.

26 **Discussion**

27 Alzheimer's disease is a neurodegenerative disorder that involves increasingly larger areas of the
28 brain over time, and has been proposed to spread along the neuronal network through defined

1 topographical patterns. Disruption of synaptic functionality and abnormal microglia function
2 have been recently identified as early mechanisms in the disease, preceding aggregate formation
3 and neuronal damage in vulnerable brain regions. However, we still lack a full understanding of
4 how synaptic dysfunction originates, propagates and is linked to microglial activation in the
5 affected brain. There is an urgent need to address these questions in order to design treatments to
6 delay Alzheimer's disease onset and/or progression, as current drugs treat symptoms,
7 temporarily helping memory and thinking problems, but do not interrupt the disease process.^{76,77}
8 In this study, we unveil a novel mechanism through which microglia contribute to the onset and
9 propagation of early synaptic dysfunction along the entorhinal-hippocampal circuit, a brain
10 region primarily affected in Alzheimer's disease. We show that large EVs, released by primary
11 microglia that have taken up A β ₄₂, locally affect dendritic spine size in cultured neurons, impair
12 synaptic plasticity in culture and brain slices and spread LTP impairment along the entorhinal-
13 hippocampal circuitry.

14 **A β exposed on EV surface accounts for synaptic dysfunction**

15 A β -EV-mediated synaptic alterations are due to their A β cargo, as only EVs carrying the peptide
16 (synthetic or naturally produced by cells) decrease dendritic spine size and impair synaptic
17 plasticity *in vitro* and *in vivo* (EC). A β -EV action perfectly mimics that of soluble oligomeric
18 A β ₄₂, which impairs LTP in EC⁶⁶ and DG⁷⁸ brain slices, acting mainly on the post-synaptic site
19 of the synapse. Specifically, patch clamp recordings from EC pyramidal cells indicate that A β -
20 EVs reduce mEPSC amplitude without affecting their frequency, as A β ₄₂ does.⁶⁵ Moreover, A β -
21 EVs shift the balance of dendritic spines towards immature structures in cultured neurons,
22 similarly to oligomeric A β ₄₂,⁷⁹ and in agreement with the findings obtained in early stage
23 Alzheimer's disease transgenic mice.⁶⁴

24 The analogy between the action of free and EV-associated A β suggests that the peptide is
25 exposed on EV surface, as previously argued.^{43,50} This would also explain the very rapid
26 conversion of dendritic protrusions to immature spines, detectable already 2 min after contact
27 with one single large A β -EV.

28 Consistent with A β externalization on large EVs, we here show that i) A β ₄₂ is detectable by
29 ELISA in large EVs in the absence of any detergent, and ii) large EVs carrying A β , that is

1 enriched in negatively charged residues,⁶⁷ exhibit a negative shift in the surface charge with
2 respect to ctrl-EVs, as indicated by TRPS analysis. Importantly, being exposed on the EV
3 surface, A β can spread post-synaptic changes through interactors present on the neuron surface
4 without the need of being transferred to the neuron cytoplasm (Fig. 8). This would explain why
5 A β -induced synaptic dysfunction largely precedes the appearance of A β deposit in Alzheimer's
6 disease affected brain.

7 Several molecules expressed on the neuron membrane are listed as A β interactors and may
8 mediate synaptic deficits induced by surface A β .⁸⁰⁻⁸³ Some of these molecules (i.e. α 7-nicotinic
9 acetylcholine receptor (α 7-nAChR), Ephrin B2 (EphB2), receptor for the advanced glycation end
10 products (RAGE), and cellular prion protein (PrP^C)) act inside dynamic signaling platforms (or
11 signalosomes) located on the post-synaptic membrane of neurons, and signal through the N-
12 methyl-D-aspartate receptor (NMDAR), therefore possibly mediating the post-synaptic effects of
13 A β -EVs.⁸¹ Their involvement in synaptic dysfunction will need further investigations.

14 Other component(s) of A β -EVs may contribute to synaptic alterations besides A β . Accordingly,
15 we show that EVs produced by classical inflammatory microglia (i-EVs), devoid of A β ,^{57,75} are
16 still capable of blocking LTP in the EC, despite not propagating synaptic dysfunction to the DG.
17 In line with this finding, the inflammatory interferon pathway has been recently shown to
18 possess a potent but incomplete capacity to drive a neurodegenerative phenotype in microglia
19 and synaptic pathology in the mouse brain.⁸⁴ Further experiments are needed to identify the
20 inflammatory molecules of i-EVs causing LTP impairment and to define their mode of action.

21 **EVs are essential vehicles for the propagation of synaptic** 22 **dysfunction**

23 A key strength of our study is the demonstration that microglial EVs are essential vehicles for the
24 spreading of A β -dependent synaptic dysfunction. Indeed, while free oligomeric A β ₄₂ is unable to
25 perturb synaptic functionality far from the injection site, packaging into EVs makes A β able to
26 spread synaptic plasticity defects along the EC-DG circuitry. Furthermore, packaging into EVs
27 makes A β effective at lower concentration compared to free soluble oligomeric A β ₄₂ (9 nM
28 active concentration of EV-associated A β ₄₂ vs 200 nM of free A β ₄₂). This is in line with previous
29 evidence showing that i) natural lipids shift the equilibrium between insoluble and soluble A β

1 toward toxic soluble species^{85,86}; ii) the lipidic EV environment favors the acquisition of
2 synaptotoxic A β conformations.⁴² Similar roles for EVs have been recently reported in tau
3 pathology.^{44,87}

4 Notably, the action of large EVs produced by microglia exposed to high concentration of
5 synthetic A β ₄₂ have been validated with EVs derived from microglia exposed to oligomeric A β
6 forms released by CHO7PA2 cells at nanomolar concentrations, in a setting which better mimics
7 microglia activation at early Alzheimer's disease stages. However, whether large EVs produced
8 endogenously by microglia may spread synaptic dysfunction in a model of Alzheimer's disease,
9 e.g. mice selectively overexpressing APP/A β in the EC,¹³ still remains unclear. Selective tools to
10 manipulate endogenous production of large EVs are needed to overcome this limitation of our
11 study and to analyze the role of large microglial EVs carrying A β in a more physiological
12 context. It should be noted, however, that large EVs carrying A β species are present in the
13 cerebrospinal fluid of Alzheimer's disease patients⁴² and their production from
14 microglia/macrophages correlates with early brain damage in prodromal Alzheimer's disease,^{42,53}
15 thus suggesting the involvement of endogenously produced large microglial EVs in Alzheimer's
16 initiation. In addition, inhibition of EV biogenesis by a brain permeant antagonist of the ATP
17 receptor P2X7 recently revealed an amelioration of disease propagation in a tauopathy mouse
18 model.⁴⁶ Despite the antagonist does not selectively block EV biogenesis in microglia, this study
19 clearly supports a role for EVs endogenously produced in the brain upon ATP stimulation in
20 disease progression.

21 Whether large EVs of other cell origin (e.g. neurons or astrocytes) can induce similar synaptic
22 dysfunction in the entorhinal-hippocampal circuit is an interesting question, worth to be
23 addressed in future experiments. Many studies have revealed a role for small-EVs released by
24 neurons or astrocytes as carriers of Alzheimer-related misfolded proteins^{51,88-93} but their impact
25 on synaptic plasticity has never been explored.

26 **EV motion at the axon surface is involved in the propagation of** 27 **synaptic dysfunction**

28 Our work indicates a novel extracellular route by which large A β -EVs move in the brain
29 parenchyma, spreading synaptic dysfunction. Previous evidence shows that small EVs storing

1 A β , isolated from Alzheimer's disease brain, can be internalized by cultured neurons and
2 intracellularly transferred between neurons through axonal projections, spreading
3 neurotoxicity.^{88,91} Our study goes well beyond these works by showing that: i) large A β -EVs,
4 which might not be transported intracellularly without impairing vesicle trafficking, move *in*
5 *vitro* at the axon surface; ii) annexin-V coating is a valid treatment to inhibit extracellular EV
6 motion. Annexin-V, bound to PS residues on EV surface, can link the EV to tether molecule(s)
7 expressed by recipient cells,⁹⁴ thus stabilizing EV-neuron contact with axons, inside which large
8 EVs cannot be internalized (this study and⁵⁴), and hampering extracellular EV motion; iii) A β -
9 EVs injected in the EC impair LTP in both the EC and the DG, while more static A β -EVs
10 (annexin-V coated) inhibit LTP only in the EC and cannot propagate LTP impairment to the DG.
11 Collectively these findings implicate extracellular motion of large A β -EVs in the propagation of
12 synaptic dysfunction in the entorhinal-hippocampal circuit. However, due to current limitation of
13 EV imaging in the mouse brain,⁹⁵ we do not provide direct evidence for extracellular A β -EV
14 motion *in vivo*. Neither we can exclude the possible contribution of small EVs to synaptic
15 alterations, given that small EVs are present in the large EV-enriched fraction injected into the
16 mouse cortex. Thus, we cannot rule out that delayed LTP impairment in the DG might be
17 secondary to some alterations induced by A β -EVs on EC layer II cells and that such changes
18 may be inhibited by annexin-V coating similarly to A β -EV motion. In future studies, translucent
19 zebrafish embryos, which allow tracking of EVs at single-vesicle level, may help to overcome
20 this limitation of our work.

21 **Exploring EV-neuron interaction dynamics**

22 The employment of optical tweezers technology combined to time lapse imaging has been
23 fundamental to study the effects of single EV on the synapse and to show for the first time that
24 one single EV (single ctrl- and A β -EV tested) is sufficient to elicit a detectable effect (dendritic
25 spine alteration) in a recipient cell. Optical manipulation experiments started from the
26 observation, during live imaging in cultures, that EVs can randomly attach not only to the soma
27 but also to the processes of neurons,⁵⁷ suggesting that this technique allows the monitoring of a
28 physiological EV-neuron interaction, difficult to be otherwise imaged. Using this approach, we
29 recently showed that astrocytic EVs move at the neuron surface with a speed similar to that

1 previously reported for small exosomes, which surf along filopodia to enter cells at endocytic hot
2 spots.⁹⁶ In addition, we showed that motion of most astrocytes-derived EVs at the neuron surface
3 is driven by the interaction of the prion protein (PrP) on EVs with its neuronal receptor(s), which
4 elicit(s) EV motion by linking EVs to a dynamic actin cytoskeleton.⁵⁴ Neuronal receptors of
5 vesicular PrP include PrP itself, that is capable to undergo homophilic interaction with PrP
6 molecule in trans,^{97,98} eliciting EV-neuron contact. Importantly, A β on the vesicular surface can
7 also interact with neuronal PrP, and this might explain why A β -EVs move more efficiently
8 compared to ctrl-EVs. However, other surface molecules of A β -EVs may control EV docking
9 and extracellular motion, e.g. intercellular adhesion molecules (ICAMs) which bind to integrins,
10 integrins themselves, lectins (e.g. galectins 1, 3) that interact with proteoglycans.^{94,99,100} All these
11 molecules, along with PrP, also stimulate neurite outgrowth¹⁰¹ and may therefore be responsible
12 for the ability of microglial EVs (both ctrl-EVs and A β -EVs) to promote formation of actin
13 protrusions, including spine-head filopodia,¹⁰² at EV-neuron contact sites, mimicking the ability
14 of parental microglia to induce spine formation at microglia-synapse contact sites.¹⁰² With
15 respect to the prevalent anterograde direction of A β -EV motion, we speculate that surface
16 proteins unique of A β -EVs may drive the interaction of A β -EVs with neuronal receptors
17 characterized by prevalent anterograde motion.

18 To conclude, a new model emerges from our study, which points to a central role for large
19 microglial EVs, carrying surface A β , in the onset and propagation of early synaptic dysfunction
20 throughout Alzheimer-specific topographical patterns (Fig. 8). Despite less studied compared
21 than small EVs (exosomes), large EVs are functionally not less relevant, and may be the target of
22 novel strategies to counteract Alzheimer's disease onset and progression.

23 **Author contributions**

24 MG performed all electrophysiological recordings and OT experiments, analyzed data, wrote the
25 original draft and prepared all figures. IP, GDA and EB contributed to analysis of EV motion. PJ
26 performed synaptic puncta analysis after EV addition in bulk and immunofluorescence analysis
27 of chemical LTP. CF and GR performed EV injection in the EC. RZ and AR contributed to
28 validation of EV preparations. FT contributed to electrophysiological recordings. OA, NO and
29 CV conceived and supervised the study and edited the manuscript.

1 **Acknowledgements**

2 We thank Arianna Chesi for helping in some experiments, Dr Paolo Swuec (University of
3 Milan, Milan, Italy) for cryo-electron microscopy analysis of EVs and Dr Dan Cojoc (CNR
4 Institute of Materials, Trieste, Italy) for help in setting the OT system.

5 **Funding**

6 This work was supported by American National Institutes of Health (NIH) 1R56AG056108-
7 01 to OA and CV-by Alzheimer's Association Research Fellowship (AARF) 2018-AARF-
8 588984 to IP, and by Italian Multiple Sclerosis Foundation (FISM) cod. 2018/R/22 and
9 financed or co-financed with the '5 per mille' public funding to CV. MG was supported by a
10 FISM senior research fellowship (cod. 2016/B/2) and financed or co-financed with the '5 per
11 mille' public funding.

12 **Competing interests**

13 OA is a founder of Neurokine Therapeutics. OA has received research funding from Appia
14 Pharmaceuticals LLC. MG, IP, GDA, PJ, CF, GR, EB, RZ, FT, AR, NO, CV report no
15 competing interests.

16 **Supplementary material**

17 Supplementary material is available at *Brain* online.

18

1 **References**

- 2 1. Selkoe DJ. Normal and abnormal biology of the beta-amyloid precursor protein. *Annu*
3 *Rev Neurosci.* 1994;17:489-517. doi:10.1146/annurev.ne.17.030194.002421
- 4 2. Salter MW, Stevens B. Microglia emerge as central players in brain disease. *Nature*
5 *medicine.* Sep 8 2017;23(9):1018-1027. doi:10.1038/nm.4397
- 6 3. Braak H, Braak E. Neuropathological staging of Alzheimer-related changes. *Acta*
7 *Neuropathol.* 1991;82(4):239-59. doi:10.1007/BF00308809
- 8 4. Thal DR, Rub U, Orantes M, Braak H. Phases of A beta-deposition in the human brain
9 and its relevance for the development of AD. *Neurology.* Jun 25 2002;58(12):1791-800.
10 doi:10.1212/wnl.58.12.1791
- 11 5. Braak H, Alafuzoff I, Arzberger T, Kretschmar H, Del Tredici K. Staging of Alzheimer
12 disease-associated neurofibrillary pathology using paraffin sections and immunocytochemistry.
13 *Acta Neuropathol.* Oct 2006;112(4):389-404. doi:10.1007/s00401-006-0127-z
- 14 6. Buckner RL, Snyder AZ, Shannon BJ, *et al.* Molecular, structural, and functional
15 characterization of Alzheimer's disease: evidence for a relationship between default activity,
16 amyloid, and memory. *J Neurosci.* Aug 24 2005;25(34):7709-17.
17 doi:10.1523/JNEUROSCI.2177-05.2005
- 18 7. Huijbers W, Mormino EC, Wigman SE, *et al.* Amyloid deposition is linked to aberrant
19 entorhinal activity among cognitively normal older adults. *J Neurosci.* Apr 9 2014;34(15):5200-
20 10. doi:10.1523/JNEUROSCI.3579-13.2014
- 21 8. Sepulcre J, Schultz AP, Sabuncu M, *et al.* In Vivo Tau, Amyloid, and Gray Matter
22 Profiles in the Aging Brain. *J Neurosci.* Jul 13 2016;36(28):7364-74.
23 doi:10.1523/JNEUROSCI.0639-16.2016
- 24 9. Selkoe DJ. Alzheimer's disease is a synaptic failure. *Science.* Oct 25
25 2002;298(5594):789-91. doi:10.1126/science.1074069
- 26 10. Selkoe DJ, Hardy J. The amyloid hypothesis of Alzheimer's disease at 25 years. *EMBO*
27 *molecular medicine.* Jun 2016;8(6):595-608. doi:10.15252/emmm.201606210
- 28 11. Masliah E, Mallory M, Alford M, *et al.* Altered expression of synaptic proteins occurs
29 early during progression of Alzheimer's disease. *Neurology.* Jan 9 2001;56(1):127-9.
30 doi:10.1212/wnl.56.1.127

- 1 12. Terry RD, Masliah E, Salmon DP, *et al.* Physical basis of cognitive alterations in
2 Alzheimer's disease: synapse loss is the major correlate of cognitive impairment. *Ann Neurol.*
3 Oct 1991;30(4):572-80. doi:10.1002/ana.410300410
- 4 13. Harris JA, Devidze N, Verret L, *et al.* Transsynaptic progression of amyloid-beta-induced
5 neuronal dysfunction within the entorhinal-hippocampal network. *Neuron.* Nov 4
6 2010;68(3):428-41. doi:10.1016/j.neuron.2010.10.020
- 7 14. DeKosky ST, Scheff SW. Synapse loss in frontal cortex biopsies in Alzheimer's disease:
8 correlation with cognitive severity. *Ann Neurol.* May 1990;27(5):457-64.
9 doi:10.1002/ana.410270502
- 10 15. Lambert MP, Barlow AK, Chromy BA, *et al.* Diffusible, nonfibrillar ligands derived
11 from Abeta1-42 are potent central nervous system neurotoxins. *Proc Natl Acad Sci U S A.* May
12 26 1998;95(11):6448-53. doi:10.1073/pnas.95.11.6448
- 13 16. Shankar GM, Li S, Mehta TH, *et al.* Amyloid-beta protein dimers isolated directly from
14 Alzheimer's brains impair synaptic plasticity and memory. *Nature medicine.* Aug
15 2008;14(8):837-42. doi:10.1038/nm1782
- 16 17. Masliah E. Mechanisms of synaptic dysfunction in Alzheimer's disease. *Histol*
17 *Histopathol.* Apr 1995;10(2):509-19.
- 18 18. Oddo S, Caccamo A, Shepherd JD, *et al.* Triple-transgenic model of Alzheimer's disease
19 with plaques and tangles: intracellular Abeta and synaptic dysfunction. *Neuron.* Jul 31
20 2003;39(3):409-21. doi:10.1016/s0896-6273(03)00434-3
- 21 19. Selkoe DJ. Soluble oligomers of the amyloid beta-protein impair synaptic plasticity and
22 behavior. *Behav Brain Res.* Sep 1 2008;192(1):106-13. doi:10.1016/j.bbr.2008.02.016
- 23 20. Walsh DM, Klyubin I, Fadeeva JV, *et al.* Naturally secreted oligomers of amyloid beta
24 protein potently inhibit hippocampal long-term potentiation in vivo. *Nature.* Apr 4
25 2002;416(6880):535-9. doi:10.1038/416535a
- 26 21. Itoh A, Akaike T, Sokabe M, *et al.* Impairments of long-term potentiation in hippocampal
27 slices of beta-amyloid-infused rats. *Eur J Pharmacol.* Oct 15 1999;382(3):167-75.
28 doi:10.1016/s0014-2999(99)00601-9
- 29 22. Eichenbaum H, Yonelinas AP, Ranganath C. The medial temporal lobe and recognition
30 memory. *Annu Rev Neurosci.* 2007;30:123-52. doi:10.1146/annurev.neuro.30.051606.094328

- 1 23. Vargha-Khadem F, Gadian DG, Watkins KE, Connelly A, Van Paesschen W, Mishkin
2 M. Differential effects of early hippocampal pathology on episodic and semantic memory.
3 *Science*. Jul 18 1997;277(5324):376-80. doi:10.1126/science.277.5324.376
- 4 24. Masdeu JC, Zubieta JL, Arbizu J. Neuroimaging as a marker of the onset and progression
5 of Alzheimer's disease. *Journal of the neurological sciences*. Sep 15 2005;236(1-2):55-64.
6 doi:10.1016/j.jns.2005.05.001
- 7 25. Wu W, Small SA. Imaging the earliest stages of Alzheimer's disease. *Current Alzheimer*
8 *research*. Dec 2006;3(5):529-39. doi:10.2174/156720506779025161
- 9 26. Stranahan AM, Mattson MP. Selective vulnerability of neurons in layer II of the
10 entorhinal cortex during aging and Alzheimer's disease. *Neural Plast*. 2010;2010:108190.
11 doi:10.1155/2010/108190
- 12 27. Miller MI, Ratnanather JT, Tward DJ, *et al*. Network Neurodegeneration in Alzheimer's
13 Disease via MRI Based Shape Diffeomorphometry and High-Field Atlasing. *Frontiers in*
14 *bioengineering and biotechnology*. 2015;3:54. doi:10.3389/fbioe.2015.00054
- 15 28. Gomez-Isla T, Price JL, McKeel DW, Jr., Morris JC, Growdon JH, Hyman BT. Profound
16 loss of layer II entorhinal cortex neurons occurs in very mild Alzheimer's disease. *J Neurosci*. Jul
17 15 1996;16(14):4491-500.
- 18 29. Scheff SW, Price DA, Schmitt FA, Mufson EJ. Hippocampal synaptic loss in early
19 Alzheimer's disease and mild cognitive impairment. *Neurobiol Aging*. Oct 2006;27(10):1372-84.
20 doi:10.1016/j.neurobiolaging.2005.09.012
- 21 30. Lazarov O, Lee M, Peterson DA, Sisodia SS. Evidence that synaptically released beta-
22 amyloid accumulates as extracellular deposits in the hippocampus of transgenic mice. *J*
23 *Neurosci*. Nov 15 2002;22(22):9785-93.
- 24 31. Sheng JG, Price DL, Koliatsos VE. Disruption of corticocortical connections ameliorates
25 amyloid burden in terminal fields in a transgenic model of Abeta amyloidosis. *J Neurosci*. Nov
26 15 2002;22(22):9794-9.
- 27 32. Lambert JC, Ibrahim-Verbaas CA, Harold D, *et al*. Meta-analysis of 74,046 individuals
28 identifies 11 new susceptibility loci for Alzheimer's disease. *Nat Genet*. Dec 2013;45(12):1452-
29 8. doi:10.1038/ng.2802

- 1 33. Zhang B, Gaiteri C, Bodea LG, *et al.* Integrated systems approach identifies genetic
2 nodes and networks in late-onset Alzheimer's disease. *Cell*. Apr 25 2013;153(3):707-20.
3 doi:10.1016/j.cell.2013.03.030
- 4 34. Guerreiro R, Wojtas A, Bras J, *et al.* TREM2 variants in Alzheimer's disease. *The New*
5 *England journal of medicine*. Jan 10 2013;368(2):117-27. doi:10.1056/NEJMoa1211851
- 6 35. Jonsson T, Stefansson H, Steinberg S, *et al.* Variant of TREM2 associated with the risk
7 of Alzheimer's disease. *The New England journal of medicine*. Jan 10 2013;368(2):107-16.
8 doi:10.1056/NEJMoa1211103
- 9 36. Efthymiou AG, Goate AM. Late onset Alzheimer's disease genetics implicates microglial
10 pathways in disease risk. *Mol Neurodegener*. May 26 2017;12(1):43. doi:10.1186/s13024-017-
11 0184-x
- 12 37. Villegas-Llerena C, Phillips A, Garcia-Reitboeck P, Hardy J, Pocock JM. Microglial
13 genes regulating neuroinflammation in the progression of Alzheimer's disease. *Curr Opin*
14 *Neurobiol*. Feb 2016;36:74-81. doi:10.1016/j.conb.2015.10.004
- 15 38. Heneka MT, Carson MJ, El Khoury J, *et al.* Neuroinflammation in Alzheimer's disease.
16 *The Lancet Neurology*. Apr 2015;14(4):388-405. doi:10.1016/S1474-4422(15)70016-5
- 17 39. Calsolaro V, Edison P. Neuroinflammation in Alzheimer's disease: Current evidence and
18 future directions. *Alzheimers Dement*. Jun 2016;12(6):719-32. doi:10.1016/j.jalz.2016.02.010
- 19 40. Welikovitsh LA, Do Carmo S, Magloczky Z, *et al.* Early intraneuronal amyloid triggers
20 neuron-derived inflammatory signaling in APP transgenic rats and human brain. *Proc Natl Acad*
21 *Sci U S A*. Mar 24 2020;117(12):6844-6854. doi:10.1073/pnas.1914593117
- 22 41. Hong S, Beja-Glasser VF, Nfonoyim BM, *et al.* Complement and microglia mediate early
23 synapse loss in Alzheimer mouse models. *Science*. May 6 2016;352(6286):712-716.
24 doi:10.1126/science.aad8373
- 25 42. Joshi P, Turola E, Ruiz A, *et al.* Microglia convert aggregated amyloid-beta into
26 neurotoxic forms through the shedding of microvesicles. *Cell Death Differ*. Apr 2014;21(4):582-
27 93. doi:10.1038/cdd.2013.180
- 28 43. Gouwens LK, Ismail MS, Rogers VA, *et al.* Abeta42 Protofibrils Interact with and Are
29 Trafficked through Microglial-Derived Microvesicles. *ACS Chem Neurosci*. Jun 20
30 2018;9(6):1416-1425. doi:10.1021/acschemneuro.8b00029

- 1 44. Asai H, Ikezu S, Tsunoda S, *et al.* Depletion of microglia and inhibition of exosome
2 synthesis halt tau propagation. *Nat Neurosci.* Nov 2015;18(11):1584-93. doi:10.1038/nn.4132
- 3 45. Crotti A, Sait HR, McAvoy KM, *et al.* BIN1 favors the spreading of Tau via extracellular
4 vesicles. *Sci Rep.* Jul 1 2019;9(1):9477. doi:10.1038/s41598-019-45676-0
- 5 46. Ruan Z, Delpech JC, Venkatesan Kalavai S, *et al.* P2RX7 inhibitor suppresses exosome
6 secretion and disease phenotype in P301S tau transgenic mice. *Mol Neurodegener.* Aug 18
7 2020;15(1):47. doi:10.1186/s13024-020-00396-2
- 8 47. Chivet M, Javalet C, Laulagnier K, Blot B, Hemming FJ, Sadoul R. Exosomes secreted
9 by cortical neurons upon glutamatergic synapse activation specifically interact with neurons. *J*
10 *Extracell Vesicles.* 2014;3:24722. doi:10.3402/jev.v3.24722
- 11 48. Koles K, Nunnari J, Korkut C, *et al.* Mechanism of evenness interrupted (Evi)-exosome
12 release at synaptic boutons. *J Biol Chem.* May 11 2012;287(20):16820-34.
13 doi:10.1074/jbc.M112.342667
- 14 49. Bianco F, Perrotta C, Novellino L, *et al.* Acid sphingomyelinase activity triggers
15 microparticle release from glial cells. *EMBO J.* Apr 22 2009;28(8):1043-54.
16 doi:10.1038/emboj.2009.45
- 17 50. Picciolini S, Gualerzi A, Carlomagno C, *et al.* An SPRi-based biosensor pilot study:
18 Analysis of multiple circulating extracellular vesicles and hippocampal volume in Alzheimer's
19 disease. *Journal of pharmaceutical and biomedical analysis.* Jan 5 2021;192:113649.
20 doi:10.1016/j.jpba.2020.113649
- 21 51. Eitan E, Hutchison ER, Marosi K, *et al.* Extracellular Vesicle-Associated Abeta Mediates
22 Trans-Neuronal Bioenergetic and Ca(2+)-Handling Deficits in Alzheimer's Disease Models. *NPJ*
23 *aging and mechanisms of disease.* 2016;2doi:10.1038/npjamd.2016.19
- 24 52. Thery C, Witwer KW, Aikawa E, *et al.* Minimal information for studies of extracellular
25 vesicles 2018 (MISEV2018): a position statement of the International Society for Extracellular
26 Vesicles and update of the MISEV2014 guidelines. *J Extracell Vesicles.* 2018;7(1):1535750.
27 doi:10.1080/20013078.2018.1535750
- 28 53. Agosta F, Dalla Libera D, Spinelli EG, *et al.* Myeloid microvesicles in cerebrospinal
29 fluid are associated with myelin damage and neuronal loss in mild cognitive impairment and
30 Alzheimer disease. *Ann Neurol.* Dec 2014;76(6):813-25. doi:10.1002/ana.24235

- 1 54. D'Arrigo G, Gabrielli M, Scaroni F, *et al.* Astrocytes-derived extracellular vesicles in
2 motion at the neuron surface: Involvement of the prion protein. *J Extracell Vesicles*. Jul
3 2021;10(9):e12114. doi:10.1002/jev2.12114
- 4 55. Gabrielli M, Battista N, Riganti L, *et al.* Active endocannabinoids are secreted on
5 extracellular membrane vesicles. *EMBO Rep*. Feb 2015;16(2):213-20.
6 doi:10.15252/embr.201439668
- 7 56. Podlisny MB, Ostaszewski BL, Squazzo SL, *et al.* Aggregation of secreted amyloid beta-
8 protein into sodium dodecyl sulfate-stable oligomers in cell culture. *J Biol Chem*. Apr 21
9 1995;270(16):9564-70. doi:10.1074/jbc.270.16.9564
- 10 57. Prada I, Gabrielli M, Turola E, *et al.* Glia-to-neuron transfer of miRNAs via extracellular
11 vesicles: a new mechanism underlying inflammation-induced synaptic alterations. *Acta*
12 *Neuropathol*. Apr 2018;135(4):529-550. doi:10.1007/s00401-017-1803-x
- 13 58. Zendrini A, Paolini L, Busatto S, *et al.* Augmented Colorimetric NANoplasmonic
14 (CONAN) Method for Grading Purity and Determine Concentration of EV Microliter Volume
15 Solutions. *Frontiers in bioengineering and biotechnology*. 2019;7:452.
16 doi:10.3389/fbioe.2019.00452
- 17 59. Bianco F, Pravettoni E, Colombo A, *et al.* Astrocyte-derived ATP induces vesicle
18 shedding and IL-1 beta release from microglia. *J Immunol*. Jun 1 2005;174(11):7268-77.
19 doi:10.4049/jimmunol.174.11.7268
- 20 60. Osteikoetxea X, Sodar B, Nemeth A, *et al.* Differential detergent sensitivity of
21 extracellular vesicle subpopulations. *Org Biomol Chem*. Oct 14 2015;13(38):9775-82.
22 doi:10.1039/c5ob01451d
- 23 61. Prada I, Amin L, Furlan R, Legname G, Verderio C, Cojoc D. A new approach to follow
24 a single extracellular vesicle-cell interaction using optical tweezers. *Biotechniques*. Jan
25 2016;60(1):35-41. doi:10.2144/000114371
- 26 62. Brenna S, Altmeppen HC, Mohammadi B, *et al.* Characterization of brain-derived
27 extracellular vesicles reveals changes in cellular origin after stroke and enrichment of the prion
28 protein with a potential role in cellular uptake. *J Extracell Vesicles*. Aug 27 2020;9(1):1809065.
29 doi:10.1080/20013078.2020.1809065
- 30 63. Origlia N, Capsoni S, Cattaneo A, *et al.* Abeta-dependent Inhibition of LTP in different
31 intracortical circuits of the visual cortex: the role of RAGE. *J Alzheimers Dis*. 2009;17(1):59-68.

- 1 64. Criscuolo C, Fontebasso V, Middei S, *et al.* Entorhinal Cortex dysfunction can be
2 rescued by inhibition of microglial RAGE in an Alzheimer's disease mouse model. *Sci Rep.* Feb
3 13 2017;7:42370. doi:10.1038/srep42370
- 4 65. Origlia N, Bonadonna C, Rosellini A, *et al.* Microglial receptor for advanced glycation
5 end product-dependent signal pathway drives beta-amyloid-induced synaptic depression and
6 long-term depression impairment in entorhinal cortex. *J Neurosci.* Aug 25 2010;30(34):11414-
7 25. doi:10.1523/JNEUROSCI.2127-10.2010
- 8 66. Origlia N, Righi M, Capsoni S, *et al.* Receptor for advanced glycation end product-
9 dependent activation of p38 mitogen-activated protein kinase contributes to amyloid-beta-
10 mediated cortical synaptic dysfunction. *J Neurosci.* Mar 26 2008;28(13):3521-30.
11 doi:10.1523/JNEUROSCI.0204-08.2008
- 12 67. Ziehm T, Brener O, van Groen T, *et al.* Increase of Positive Net Charge and
13 Conformational Rigidity Enhances the Efficacy of d-Enantiomeric Peptides Designed to
14 Eliminate Cytotoxic Abeta Species. *ACS Chem Neurosci.* Aug 17 2016;7(8):1088-96.
15 doi:10.1021/acschemneuro.6b00047
- 16 68. Kasai H, Matsuzaki M, Noguchi J, Yasumatsu N, Nakahara H. Structure-stability-
17 function relationships of dendritic spines. *Trends Neurosci.* Jul 2003;26(7):360-8.
18 doi:10.1016/S0166-2236(03)00162-0
- 19 69. Lu W, Man H, Ju W, Trimble WS, MacDonald JF, Wang YT. Activation of synaptic
20 NMDA receptors induces membrane insertion of new AMPA receptors and LTP in cultured
21 hippocampal neurons. *Neuron.* Jan 2001;29(1):243-54. doi:10.1016/s0896-6273(01)00194-5
- 22 70. Fossati G, Morini R, Corradini I, *et al.* Reduced SNAP-25 increases PSD-95 mobility and
23 impairs spine morphogenesis. *Cell Death Differ.* Sep 2015;22(9):1425-36.
24 doi:10.1038/cdd.2014.227
- 25 71. Antonucci F, Turola E, Riganti L, *et al.* Microvesicles released from microglia stimulate
26 synaptic activity via enhanced sphingolipid metabolism. *EMBO J.* Mar 7 2012;31(5):1231-40.
27 doi:10.1038/emboj.2011.489
- 28 72. Bliss TV, Collingridge GL. A synaptic model of memory: long-term potentiation in the
29 hippocampus. *Nature.* Jan 7 1993;361(6407):31-9. doi:10.1038/361031a0
- 30 73. Liu L, Drouet V, Wu JW, *et al.* Trans-synaptic spread of tau pathology in vivo. *PLoS*
31 *One.* 2012;7(2):e31302. doi:10.1371/journal.pone.0031302

- 1 74. Tamamaki N, Nojyo Y. Projection of the entorhinal layer II neurons in the rat as revealed
2 by intracellular pressure-injection of neurobiotin. *Hippocampus*. Oct 1993;3(4):471-80.
3 doi:10.1002/hipo.450030408
- 4 75. Lombardi M, Parolisi R, Scaroni F, *et al.* Detrimental and protective action of microglial
5 extracellular vesicles on myelin lesions: astrocyte involvement in remyelination failure. *Acta*
6 *Neuropathol*. Dec 2019;138(6):987-1012. doi:10.1007/s00401-019-02049-1
- 7 76. Yiannopoulou KG, Papageorgiou SG. Current and future treatments for Alzheimer's
8 disease. *Ther Adv Neurol Disord*. Jan 2013;6(1):19-33. doi:10.1177/1756285612461679
- 9 77. Godyn J, Jonczyk J, Panek D, Malawska B. Therapeutic strategies for Alzheimer's
10 disease in clinical trials. *Pharmacol Rep*. Feb 2016;68(1):127-38.
11 doi:10.1016/j.pharep.2015.07.006
- 12 78. Wang H-W, Pasternak JF, Kuo H, *et al.* Soluble oligomers of beta amyloid (1-42) inhibit
13 long-term potentiation but not long-term depression in rat dentate gyrus. *Brain Res*.
14 2002;924(2):133-40.
- 15 79. Palop JJ, Mucke L. Amyloid-beta-induced neuronal dysfunction in Alzheimer's disease:
16 from synapses toward neural networks. *Nat Neurosci*. Jul 2010;13(7):812-8.
17 doi:10.1038/nn.2583
- 18 80. De Strooper B, Karran E. The Cellular Phase of Alzheimer's Disease. *Cell*. Feb 11
19 2016;164(4):603-15. doi:10.1016/j.cell.2015.12.056
- 20 81. Jarosz-Griffiths HH, Noble E, Rushworth JV, Hooper NM. Amyloid-beta Receptors: The
21 Good, the Bad, and the Prion Protein. *J Biol Chem*. Feb 12 2016;291(7):3174-83.
22 doi:10.1074/jbc.R115.702704
- 23 82. Mroczko B, Groblewska M, Litman-Zawadzka A, Kornhuber J, Lewczuk P. Cellular
24 Receptors of Amyloid beta Oligomers (AbetaOs) in Alzheimer's Disease. *Int J Mol Sci*. Jun 27
25 2018;19(7)doi:10.3390/ijms19071884
- 26 83. Arancio O, Zhang HP, Chen X, *et al.* RAGE potentiates Abeta-induced perturbation of
27 neuronal function in transgenic mice. *EMBO J*. Oct 13 2004;23(20):4096-105.
28 doi:10.1038/sj.emboj.7600415
- 29 84. Roy ER, Wang B, Wan YW, *et al.* Type I interferon response drives neuroinflammation
30 and synapse loss in Alzheimer disease. *J Clin Invest*. Apr 1 2020;130(4):1912-1930.
31 doi:10.1172/JCI133737

- 1 85. Martins IC, Kuperstein I, Wilkinson H, *et al.* Lipids revert inert Abeta amyloid fibrils to
2 neurotoxic protofibrils that affect learning in mice. *EMBO J.* Jan 9 2008;27(1):224-33.
3 doi:10.1038/sj.emboj.7601953
- 4 86. Johansson AS, Garlind A, Berglind-Dehlin F, *et al.* Docosahexaenoic acid stabilizes
5 soluble amyloid-beta protofibrils and sustains amyloid-beta-induced neurotoxicity in vitro. *The*
6 *FEBS journal.* Feb 2007;274(4):990-1000. doi:10.1111/j.1742-4658.2007.05647.x
- 7 87. Ruan Z, Pathak D, Venkatesan Kalavai S, *et al.* Alzheimer's disease brain-derived
8 extracellular vesicles spread tau pathology in interneurons. *Brain : a journal of neurology.* Feb
9 12 2021;144(1):288-309. doi:10.1093/brain/awaa376
- 10 88. Wang Y, Balaji V, Kaniyappan S, *et al.* The release and trans-synaptic transmission of
11 Tau via exosomes. *Mol Neurodegener.* Jan 13 2017;12(1):5. doi:10.1186/s13024-016-0143-y
- 12 89. Chiarini A, Armato U, Gardenal E, Gui L, Dal Pra I. Amyloid beta-Exposed Human
13 Astrocytes Overproduce Phospho-Tau and Overrelease It within Exosomes, Effects Suppressed
14 by Calcilytic NPS 2143-Further Implications for Alzheimer's Therapy. *Frontiers in*
15 *neuroscience.* 2017;11:217. doi:10.3389/fnins.2017.00217
- 16 90. Guix FX, Corbett GT, Cha DJ, *et al.* Detection of Aggregation-Competent Tau in
17 Neuron-Derived Extracellular Vesicles. *Int J Mol Sci.* Feb 27
18 2018;19(3)doi:10.3390/ijms19030663
- 19 91. Sardar Sinha M, Ansell-Schultz A, Civitelli L, *et al.* Alzheimer's disease pathology
20 propagation by exosomes containing toxic amyloid-beta oligomers. *Acta Neuropathol.* Jul
21 2018;136(1):41-56. doi:10.1007/s00401-018-1868-1
- 22 92. Sollvander S, Nikitidou E, Brolin R, *et al.* Accumulation of amyloid-beta by astrocytes
23 result in enlarged endosomes and microvesicle-induced apoptosis of neurons. *Mol*
24 *Neurodegener.* May 12 2016;11(1):38. doi:10.1186/s13024-016-0098-z
- 25 93. Beretta C, Nikitidou E, Streubel-Gallasch L, Ingelsson M, Sehlin D, Erlandsson A.
26 Extracellular vesicles from amyloid-beta exposed cell cultures induce severe dysfunction in
27 cortical neurons. *Sci Rep.* Nov 12 2020;10(1):19656. doi:10.1038/s41598-020-72355-2
- 28 94. van Niel G, D'Angelo G, Raposo G. Shedding light on the cell biology of extracellular
29 vesicles. *Nat Rev Mol Cell Biol.* Apr 2018;19(4):213-228. doi:10.1038/nrm.2017.125
- 30 95. Verweij FJ, Hyenne V, Van Niel G, Goetz JG. Extracellular Vesicles: Catching the Light
31 in Zebrafish. *Trends in cell biology.* Oct 2019;29(10):770-776. doi:10.1016/j.tcb.2019.07.007

- 1 96. Heusermann W, Hean J, Trojer D, *et al.* Exosomes surf on filopodia to enter cells at
2 endocytic hot spots, traffic within endosomes, and are targeted to the ER. *J Cell Biol.* Apr 25
3 2016;213(2):173-84. doi:10.1083/jcb.201506084
- 4 97. Amin L, Nguyen XT, Rolle IG, *et al.* Characterization of prion protein function by focal
5 neurite stimulation. *J Cell Sci.* Oct 15 2016;129(20):3878-3891. doi:10.1242/jcs.183137
- 6 98. Nguyen XTA, Tran TH, Cojoc D, Legname G. Copper Binding Regulates Cellular Prion
7 Protein Function. *Mol Neurobiol.* Sep 2019;56(9):6121-6133. doi:10.1007/s12035-019-1510-9
- 8 99. French KC, Antonyak MA, Cerione RA. Extracellular vesicle docking at the cellular
9 port: Extracellular vesicle binding and uptake. *Semin Cell Dev Biol.* Jul 2017;67:48-55.
10 doi:10.1016/j.semcdb.2017.01.002
- 11 100. Buzas EI, Toth EA, Sodar BW, Szabo-Taylor KE. Molecular interactions at the surface
12 of extracellular vesicles. *Semin Immunopathol.* Sep 2018;40(5):453-464. doi:10.1007/s00281-
13 018-0682-0
- 14 101. Arab T, Raffo-Romero A, Van Camp C, *et al.* Proteomic characterisation of leech
15 microglia extracellular vesicles (EVs): comparison between differential ultracentrifugation and
16 Optiprep density gradient isolation. *J Extracell Vesicles.* 2019;8(1):1603048.
17 doi:10.1080/20013078.2019.1603048
- 18 102. Weinhard L, di Bartolomei G, Bolasco G, *et al.* Microglia remodel synapses by
19 presynaptic trogocytosis and spine head filopodia induction. *Nat Commun.* Mar 26
20 2018;9(1):1228. doi:10.1038/s41467-018-03566-5
- 21 103. Polanco JC, Li C, Durisic N, Sullivan R, Gotz J. Exosomes taken up by neurons hijack
22 the endosomal pathway to spread to interconnected neurons. *Acta neuropathologica*
23 *communications.* Feb 15 2018;6(1):10. doi:10.1186/s40478-018-0514-4

24
25

1 **Figure legends**

2 **Figure 1 Morphological features and A β ₄₂ content of A β -EVs in the 10 000xg pellet**

3 **(A)** Western blot analysis for the EV markers flotillin I, alix and annexin-A2, the Golgi and
4 mitochondria markers GS28 and TOM20, the cytosolic marker GAPDH and for A β (6E10) of
5 EVs in the 10 000xg pellet from 10x10⁶ microglia and relative donor cells (2 μ g cell lysate).
6 Normalization to total proteins is shown in Supplementary Figure 1. **(B)** Analysis of the purity of
7 EV preparations from A β ₄₂-treated-microglia and control cells using the CONAN assay; AI % is
8 the relative aggregation index of gold nanoparticles (AuNP), normREF is a sample of
9 monodispersed AuNPs, negREF (HPLC grade water + AuNPs + PBS solution) is the negative
10 control threshold, and posREF is the positive control (PBS solution + AuNPs). **(C)** Size
11 distribution of large A β -EVs enriched fraction analyzed by TRPS. The fraction of A β -EVs
12 having diameter >200 nm represents ~59% of the 10 000xg pellet. **(D)** Charge measurements of
13 large ctrl-EVs and A β -EVs (10 000xg pellet) by TRPS. Ctrl-EVs display an averaged surface
14 charge of -10.75 mV, while A β -EVs of -22.57 mV (t-test, $p < 0.001$). **(E)** A β ₄₂ content in intact
15 A β -EVs or A β -EVs lysed with 0.57% Triton X-100 (10 000xg pellet), as detected by ELISA.
16 Values are normalized to intact A β -EVs. (t-test, $p = 0.002$, $n = 3$). **(F)** A β ₄₂ content in large A β -
17 EVs enriched fraction (10 000xg pellet) produced by microglia exposed for 20 h to A β ₄₂ with or
18 without Bafilomycin A1 (Baf) during the last 15 h of treatment, as detected by ELISA in the
19 presence of 0.57% Triton X-100. Values are normalized to the condition without Bafilomycin
20 (Mann-Whitney Rank Sum Test, $p < 0.001$, $n = 7$). **(G)** A β -EVs in the 10 000xg pellet from
21 microglia stimulated as in F. Values (EV numbers) are normalized to the condition without
22 Bafilomycin (Baf). (Mann-Whitney Rank Sum Test, $p = 0.908$, $n = 3$). **(H)** Representative cryo-
23 electron microscopy micrograph of ctrl- and A β -EVs in the 10 000xg pellet. Arrows point to
24 multilamellar EVs; black arrowheads to EVs with rough surface; white arrowhead to tubular
25 vesicles. Scale bars: 100 nm. Box plots show the median (central line) and mean (X), upper and
26 lower quartile (box limits), max and min values (whiskers).

1 **Figure 2 Large A β -EVs alter dendritic spine morphology and synaptic plasticity in**
 2 **cultured neurons**

3 **(A)** Schematic representation of EV delivery by optical tweezers to RFP expressing dendrite,
 4 preceded and followed by time-lapse imaging of RFP-positive dendritic spines. A z-stack of
 5 RFP-positive dendrite was first acquired with a spinning disk microscope, then a low amount of
 6 EVs was added to the cell medium and one EV was captured (trapped) above the neurons by the
 7 IR laser tweezers and placed in contact with the imaged dendrite (bright field). After 30 seconds
 8 the laser was switched off, EV adhesion was checked and confocal images were collected at the
 9 indicated time points. **(B)** Representative confocal images taken before and 30 min after contact
 10 of ctrl-EVs (center) or A β -EVs (right) following the procedure described in A, showing dendritic
 11 spine changes in proximity (top) and far from EV contact site (bottom). Red and orange circles
 12 indicate the site of EV contact. White arrows point to newly generated protrusions. Red arrows
 13 point to enlarged spines. Orange arrows point to thinned spines. On the left, dendritic spine
 14 images at 0 and 30 min after vehicle addition. Scale bar: 10 μ m. **(C-D)** Temporal analysis of
 15 dendritic spine density around the contact site (<7 μ m, C) and far from the contact site (>60 μ m,
 16 D) ($n=6$ dendrites/condition, 12 experiments). Values are normalized to the pre-adhesion
 17 condition. (Two Way RM ANOVA, followed by Holm-Sidak method; *close to the contact site:*
 18 $p=0.013$ ctrl-EVs vs. vehicle; $p<0.001$ A β -EVs 30 and 40 min vs. 0; *far from the contact site:*
 19 $p=0.937$). **(E-H)** Temporal analysis of the density of immature (thin) and mature (mushroom and
 20 stubby) dendritic spines around the contact site (E,G) and far from the contact site (F,H) after
 21 adhesion of A β -EVs or ctrl-EVs or in vehicle-treated neurons (*immature spines at the contact*
 22 *site:* $p<0.01$ A β -EVs vs. ctrl-EVs and vs. vehicle; $p<0.001$ A β -EVs 20, 30, 40 min vs. 0;
 23 *immature spines far from the contact site:* $p=0.656$; *mature spines at the contact site:* $p<0.001$
 24 A β -EVs vs. ctrl-EVs; $p=0.015$ A β -EVs vs. vehicle; $p<0.01$ ctrl-EVs vs. vehicle; $p<0.001$ ctrl-
 25 EVs 20, 30, 40 min vs. 0; *mature spines far from the contact site, ns*). **(I)** Representative images
 26 showing Shank-2/Bassoon double positive puncta in vehicle-treated neurons, neurons exposed to
 27 ctrl-EVs or A β -EVs. Scale bar: 1 μ m. **(J)** The box plot shows the corresponding fraction of
 28 juxtaposed pre- and post-synaptic puncta relative to Bassoon positive synaptic puncta (Kruskal-
 29 Wallis One Way Analysis of Variance on Ranks, followed by Dunn's method, $p<0.05$ A β -EVs
 30 vs. vehicle; $n=3$ experiments). Box plot shows the median (central line) and mean (X), upper and
 31 lower quartile (box limits), max and min values (whiskers). **(K)** Representative traces of

1 mEPSCs recorded from control neurons (vehicle) and neurons exposed to A β -EVs or ctrl-EVs
 2 for 1 h, before and after induction of synaptic plasticity. Vertical scale bar: 5 pA; Horizontal
 3 scale bar: 1 s. **(L)** Temporal plot of mEPSC frequency changes showing that glycine (Gly, 200
 4 μ M 3 min in 0 Mg⁺⁺, preceded by 1 min 0 Mg⁺⁺) induced a long lasting increase in mEPSC
 5 frequency in both vehicle and ctrl-EV treated neurons but not in neurons exposed to A β -EVs for
 6 1 h (Two Way RM ANOVA, followed by Holm-Sidak method; 2.931 ± 0.808 “vehicle” fold
 7 change from baseline, $p=0.002$; 2.409 ± 0.549 “ctrl-EVs” fold change from baseline, $p=0.027$;
 8 0.942 ± 0.156 “A β -EVs” fold change from baseline, $p=0.902$; vehicle vs. A β -EVs, $p=0.012$; ctrl-
 9 EVs vs. A β -EVs post Gly, $p=0.009$; vehicle, $n=6$ cells; ctrl-EVs, $n=5$; A β -EVs, $n=8$; 7
 10 experiments). Data are expressed as mean \pm SEM.

11 **Figure 3 Large A β -EV motion at the axon surface**

12 **(A)** Schematic representation of large EV delivery to axons through optical tweezers. Axons
 13 were selected based on their morphology after RFP transfection. A single EV was trapped by the
 14 laser tweezers in bright field and placed in contact with the axon. The trapping laser was
 15 switched off 30 seconds after contact and EV-axon interaction was monitored in bright field
 16 time-lapse for 40 min. **(B)** Sequence of phase contrast images of a large EV moving
 17 anterogradely along the axon towards the growth cone. **(B')** Corresponding fluorescence image
 18 of the axon in B. The top right blurred area indicates the region of the growth cone outside phase
 19 contrast images. **(C)** Trajectory of the EV in B superimposed to the phase contrast image. **(D)**
 20 Trajectory of a static EV superimposed to the phase contrast image. **(E)** Percentage of large ctrl-
 21 EVs and A β -EVs that adhered to axons (chi-square test, $p=0.768$, $n=68$ ctrl-EVs, $n=105$ A β -
 22 EVs, 33 experiments). **(F)** Percentage of large ctrl-EVs and A β -EVs that displayed motility on
 23 axons (chi-square, $p=0.002$, $n=29$ ctrl-EVs, $n=34$ A β -EVs, 31 experiments). **(G)** Average speed
 24 of large A β -EVs and ctrl-EVs (Mann-Whitney Test, $p=0.011$, $n=8$ ctrl-EVs, $n=18$ A β -EVs, 19
 25 experiments). **(H-I)** Pathlength (H) and max distance from the contact point in both direction (I)
 26 reached by large ctrl-EVs and A β -EVs in 10 min (Mann-Whitney, $p=0.033$, for both; $n=8$ ctrl-
 27 EVs, $n=13$ A β -EVs, 19 experiments). **(J)** Anterograde and retrograde motion of large A β -EVs
 28 and ctrl-EVs ($n=15$). **(K)** Percentage of large A β -EVs and A β -EVs pre-coated with annexin-V
 29 (coated A β -EVs, c-A β -EVs) that adhered to axons (chi-square, $p=0.014$, $n=105$ A β -EVs, $n=37$
 30 c-A β -EVs, 24 experiments). **(L)** Percentage of large A β -EVs and c-A β -EVs that displayed
 31 motility (chi-square, $p=0.002$; $n=34$ A β -EVs, $n=25$ c-A β -EVs, 23 experiments). **(M)** Average

1 speed of large A β -EVs and c-A β -EVs (t-test, $p=0.142$, $n=18$ A β -EVs, $n=11$ c-A β -EVs, 16
 2 experiments). Scale bars: 10 μ m. Percentage values are raw percentages over total EV tested.
 3 Box plots show the median (central line) and mean (X), upper and lower quartile (box limits),
 4 max and min values (whiskers).

5 **Figure 4 Large A β -EVs propagate LTP impairment in the EC-DG circuit**

6 **(A)** Input-output curves showing the relative amplitude (% maximal Ampl.) as a function of
 7 stimulus intensity (Stim.Int., measured in volts (V)) in vehicle treated slices and slices exposed
 8 to 1×10^8 /ml A β -EVs, ctrl-EVs or vehicle for 1 h. **(B)** LTP field potential recordings in slices
 9 incubated with A β -EVs (same amount as in A, yellow triangles), ctrl-EVs (dark blue circles) or
 10 vehicle alone with no EVs (light blue diamonds). LTP was reliably elicited in slices incubated
 11 with ctrl-EVs (Two-way RM ANOVA, followed by Holm-Sidak method, ctrl-EVs $131 \pm 4\%$ of
 12 baseline amplitude 40 min after HFS ($n=7$ slices, 4 mice); vehicle $134 \pm 7\%$ ($n=6$ slices, 4
 13 mice); $p=0.473$ ctrl-EVs vs vehicle), while was not elicited in A β -EVs treated EC slices ($93 \pm$
 14 3% of baseline after HFS, $p=0.154$ vs. baseline; $p<0.001$ vs. vehicle and ctrl-EVs; $n=6$ slices; 4
 15 mice). **(C)** Experimental protocol for LTP measurements in EC-DG slices after large EVs or
 16 A β_{42} injection. Large A β -EVs, ctrl-EVs or i-EVs ($0,25 \times 10^8$ EVs/ μ l, 1 μ l), A β_{42} (1 μ l, 100 nM) or
 17 vehicle were injected into the mouse lateral EC. Mice were sacrificed 1 h and 24 h after the
 18 injection and horizontal slices containing both the EC and the hippocampus have been cut. LTP
 19 was recorded from the EC superficial layer II (stimulus and recording pipette in this layer) and at
 20 the synapse between the PP (stimulus) and the DG (recording). **(D-E)** LTP plots from the EC
 21 superficial layer II (D) and the PP-DG synapse (E) in cortico-hippocampal slices after injection
 22 of large A β -EVs in the lateral EC or large ctrl-EVs in the contralateral EC. Field recordings in
 23 EC superficial layer II revealed suppression of LTP 1 h after the injection of A β -EVs in the
 24 ipsilateral EC (D, yellow triangles), while a stable LTP was recorded in the contralateral EC
 25 injected with ctrl-EVs (D, dark blue circles) (ctrl-EVs $129 \pm 6\%$ vs. A β -EVs $99 \pm 5\%$, $p<0.001$,
 26 $n=8$ slices, 4 mice each). 24 h after the injection of A β -EVs, LTP was still impaired in EC (D,
 27 orange squares) (A β -EVs $101 \pm 2\%$, $p<0.001$ vs. ctrl EVs, $n=7$ slices, 4 mice). In field
 28 recordings from the DG after PP stimulation (E), LTP was normal 1 h after the injection of A β -
 29 EVs in the EC (E, yellow triangles) and comparable to that obtained in the contralateral
 30 hippocampus injected in the EC with ctrl-EVs (E, dark blue circles) (A β -EVs $159 \pm 5\%$ vs. ctrl-
 31 EVs $147 \pm 12\%$, $p=0.195$, $n=8$ slices, 4 mice each). In contrast, LTP was blocked 24 h after A β -

1 EV injection in the ipsilateral EC (E, orange squares) ($A\beta$ -EVs $105 \pm 8\%$ $p < 0.001$ vs. ctrl EVs
 2 and $A\beta$ -EVs at 1 h, $n=7$ slices, 4 mice). **(F-G)** Effect of the stereotaxic injection of oligomeric
 3 $A\beta_{42}$ in EC on LTP expression in cortico-hippocampal slices. Field recordings in EC revealed
 4 that LTP expression is affected 1 h after the injection of $A\beta_{42}$ in the EC (F, light blue diamonds)
 5 ($93 \pm 7\%$, $p=0.187$ vs. baseline, $n=7$ slices, 4 mice) but it recovers 24 h after $A\beta_{42}$ injection (F,
 6 dark blue diamonds). Slice recordings from the DG after PP stimulation revealed that
 7 hippocampal LTP is normally expressed 1 h after the injection of $A\beta_{42}$ in the EC (G, light blue
 8 diamonds) ($176 \pm 4\%$, $n=7$ slices, 4 mice) and comparable to that obtained in hippocampal slices
 9 24 h after the injection of $A\beta_{42}$ in the EC (G, dark blue diamonds) ($176 \pm 2\%$, $p=0.039$ vs. 1 h,
 10 $n=7$ slices, 4 mice). **(H-I)** Effect of the stereotaxic injection of i-EVs in the EC on LTP
 11 expression in EC-hippocampal slices. Field recordings in EC revealed that LTP expression is
 12 affected already 1 h after i-EVs injection (H, dark gray diamonds) (i-EVs $87 \pm 4\%$ of baseline
 13 amplitude after HFS vs. ctrl-EVs $130 \pm 6\%$, $p < 0.001$, $n=8$ slices, 4 mice each) and remained
 14 impaired 24 h after (H, light gray diamonds) ($96 \pm 6\%$ of baseline amplitude, $n=6$ slices, 4 mice;
 15 $p < 0.001$ vs. ctrl-EVs and $p=0.120$ vs. i-EVs at 1 h). Hippocampal LTP was normally expressed
 16 24 h after the injection of i-EVs in the EC (I, light gray diamonds) and comparable to that
 17 obtained in hippocampal slices after the injection of ctrl-EVs in the EC (I, dark blue circles)
 18 (mean LTP was $157 \pm 11\%$ of baseline fEPSP slope, $p=0.469$ vs. ctrl-EVs $159 \pm 9\%$, $n=7$
 19 slices, 4 mice each). Inserts show representative traces of field potential. Vertical scale bar: 0.5
 20 mV; Horizontal scale bar: 5 ms. Values are mean \pm SEM.

21 **Figure 5 $A\beta$ -EVs decrease mEPSC amplitude without affecting their frequency**

22 **(A)** Experimental protocol for whole-cell patch-clamp recordings in EC-DG slices after $A\beta$ -EV
 23 (0.25×10^8 EVs/ μ l, 1 μ l) or vehicle injection. Recording electrodes are shown. **(B-C)**
 24 Representative traces of mEPSCs recorded from pyramidal cells of EC superficial layer II 1 h
 25 after injection of $A\beta$ -EVs or vehicle in the EC (B) and corresponding plots of mEPSC frequency
 26 and amplitude (C) (mEPSC frequency, t-test, $p=0.900$; mEPSC amplitude, Mann-Whitney Rank
 27 Sum Test, $p \leq 0.001$; vehicle, $n=13$ cells; $A\beta$ -EVs, $n=13$ cells; 7 mice each). **(D-E)**
 28 Representative traces of mEPSCs recorded from granular cells of the DG 24 h after injection of
 29 $A\beta$ -EVs or vehicle in the EC (D). The plots show corresponding mEPSC frequency and
 30 amplitude (E) (mEPSC frequency, t-test, $p=0.655$; mEPSC amplitude, t-test, $p \leq 0.001$; vehicle,
 31 $n=12$ cells; $A\beta$ -EVs, $n=13$ cells; 6 mice each). Vertical scale bar: 5 pA; Horizontal scale bar: 1 s.

1 Box plots show the median (central line) and mean (X) values, upper and lower quartile (box
2 limits), max and min values (whiskers).

3 **Figure 6 CHO-EVs propagate LTP impairment in the EC-DG circuit**

4 (A) Living mouse microglia were exposed to CHO7PA2 cell supernatant, containing nanomolar
5 concentration of A β , for 20 h and stained with IB4-Alexa568 to label the cell surface before
6 being fixed and counterstained with anti-A β antibody 6E10. Scale bar: 10 μ m. (B-C) Effect on
7 LTP expression of the stereotaxic injection in the EC of EVs released by microglia exposed for
8 20 h to CHO7PA2 cell supernatant (CHO-EVs, $0,25 \times 10^8$ EVs/ μ l, 1 μ l), compared to a same
9 amount of ctrl-EVs. LTP plots are relative to recordings from EC and PP-DG, 1 h and 24 h after
10 the injection respectively. (Two-way RM ANOVA, followed by Holm-Sidak method, 1 h EC:
11 85.48 ± 13.09 %, $p=0.234$ vs. baseline; $p=0.023$ vs. ctrl-EVs; $n=4$ slices CHO-EVs; $n=6$ slices
12 ctrl-EVs; 24 h PP-DG: 97.29 ± 10.86 %, $p=0.802$ vs. baseline; $p<0.01$ vs. ctrl-EVs; $n=4$ slices
13 CHO-EVs; $n=6$ slices ctrl-EVs). Vertical scale bar: 0.5 mV; Horizontal scale bar: 5 ms. Values
14 are mean \pm SEM.

15 **Figure 7 A β -EVs coated with annexin-V do not propagate LTP impairment in the EC-DG** 16 **circuit**

17 (A-B) Effect of the stereotaxic injection of A β -EVs or coated A β -EVs (c-A β -EVs) ($0,11 \times 10^8$
18 EVs/ μ l, 1 μ l) in the EC on LTP expression in EC and PP-DG, 1 h and 24 h after the injection
19 respectively. c-A β -EVs impaired LTP in EC 1 h after the injection (A) (Two-way RM ANOVA,
20 followed by Holm-Sidak method, 97.95 ± 11.19 %, $p=0.820$ vs. baseline; $p=0.152$ vs. A β -EVs;
21 $n=8$ slices ctrl-EVs; $n=6$ slices A β -EVs; $n=7$ slices c-A β -EVs; 4 mice), while allow its
22 expression in the DG 24 h later (B) (137.80 ± 5.64 %, $p=0.008$ vs. baseline; $p<0.001$ vs. A β -EVs;
23 $n=8$ slices ctrl-EVs; $n=8$ slices A β -EVs; $n=6$ slices c-A β -EVs; 5 mice). Inserts show a
24 representative trace of field potential. Vertical scale bar: 0.5 mV; Horizontal scale bar: 5 ms.
25 Values are mean \pm SEM.

26 **Figure 8 Model for synaptic dysfunction propagation mediated by large A β -EVs in** 27 **Alzheimer's disease**

28 We propose the following model to explain A β -EV implication in the onset and propagation of
29 synaptic dysfunction. In the early stages of Alzheimer's disease, A β starts to accumulate in

1 specific areas of the brain, where it is internalized by microglia (1) and re-secreted in toxic form
2 in association with EVs (2): the higher the A β cell load, the higher the A β content (as indicated
3 by Bafilomycin experiments showed in this paper). A β -EVs induce synaptic alterations at the site
4 of adhesion (3) and, by moving along axonal projection (4), can reach connected neurons (5).
5 While small EVs are internalized by neurons and travel inside neuronal axons to trans-
6 synaptically transfer their cargo (so far reported for small EVs released by primary neurons or
7 isolated from Alzheimer patients' brains),^{88,91,103} large EVs, likely too big to be transported
8 intracellularly, move at the axonal surface towards synaptically connected cells.

9

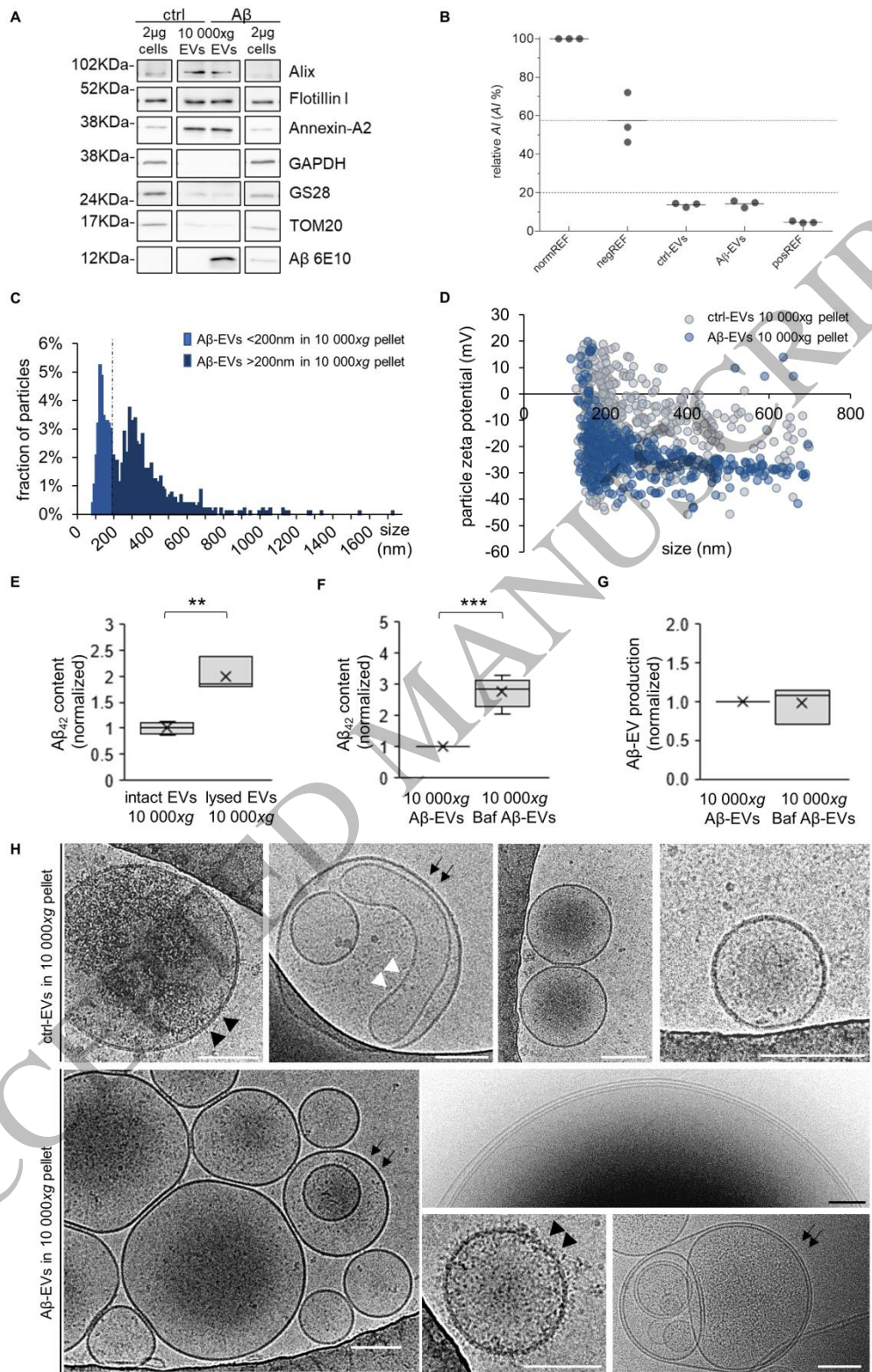


Fig. 1

1
2
3

Figure 1
190x300 mm (5.0 x DPI)

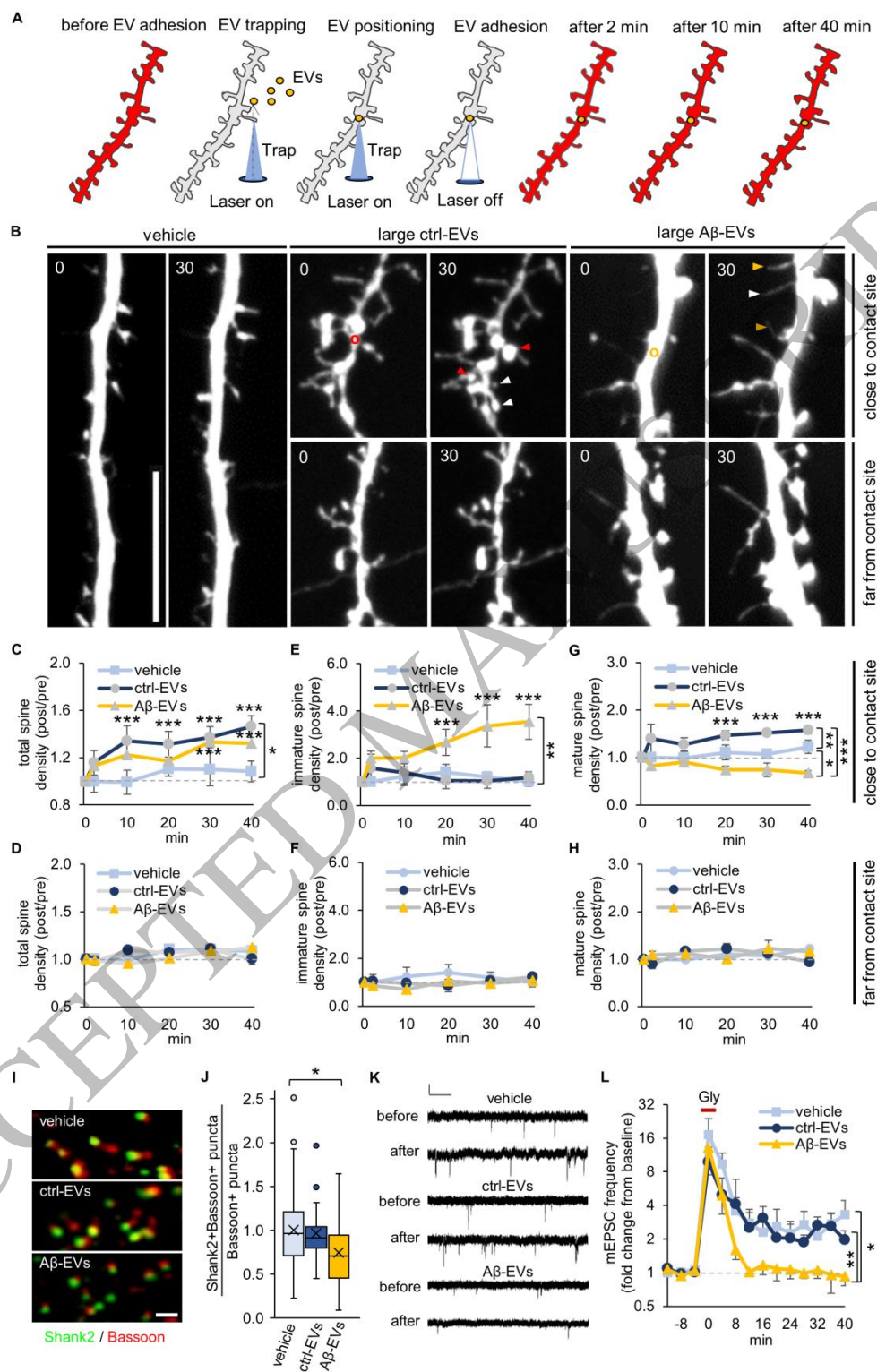


Fig. 2

Figure 2
190x310 mm (5.0 x DPI)

1
2
3

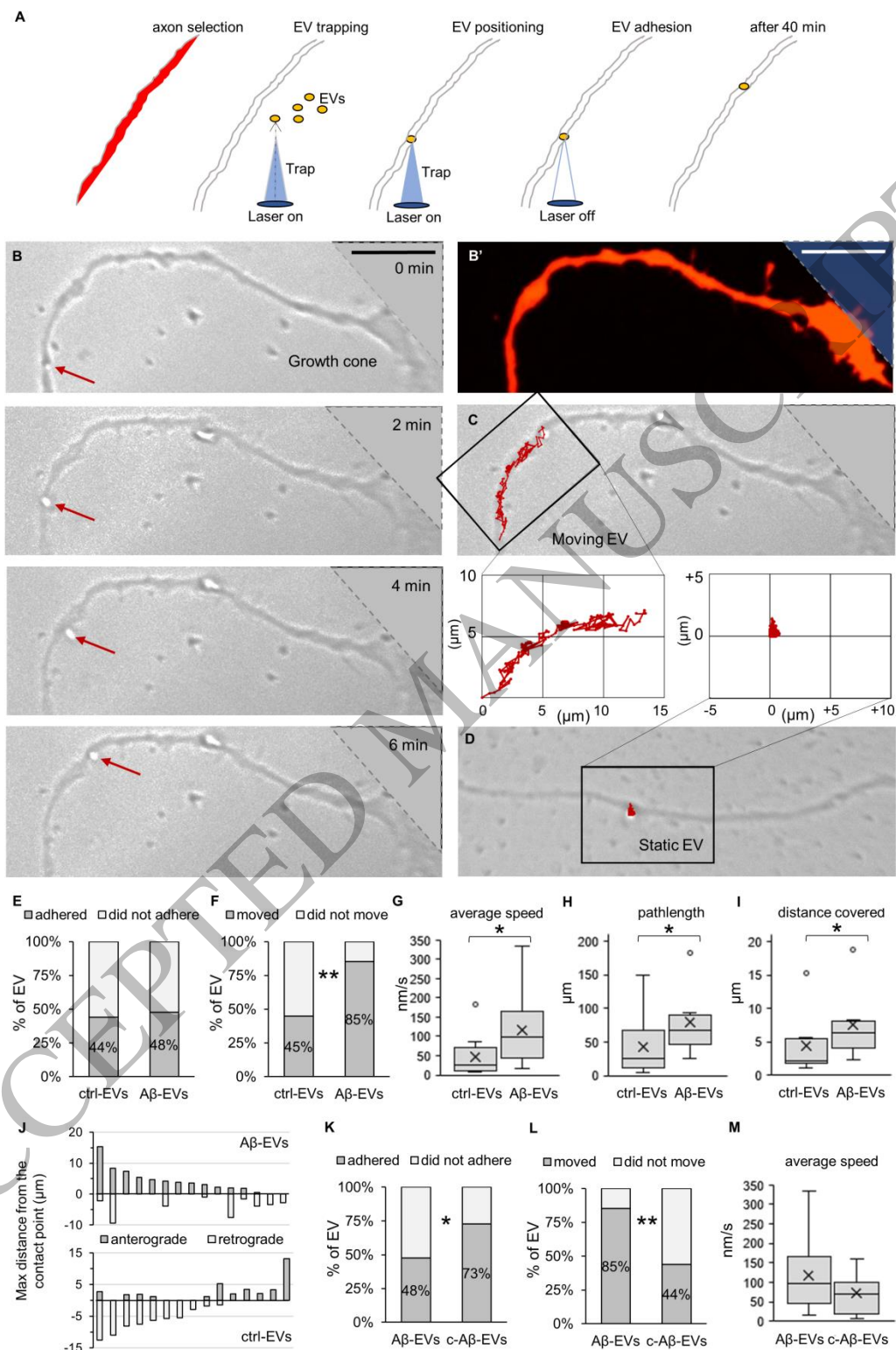


Fig. 3

Figure 3
210x320 mm (5.0 x DPI)

1
2
3

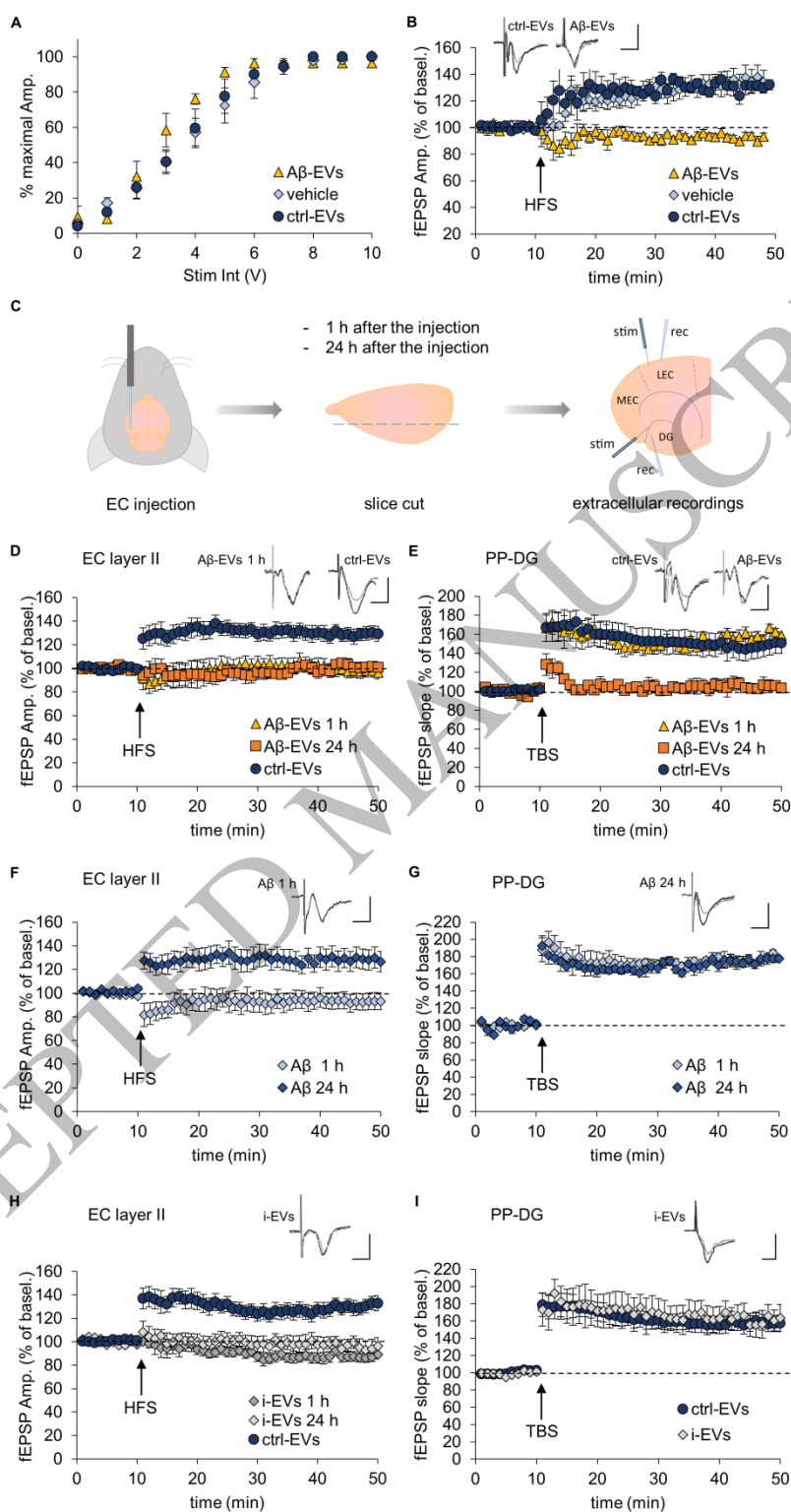


Fig. 4

Figure 4
190x339 mm (5.0 x DPI)

1
2
3

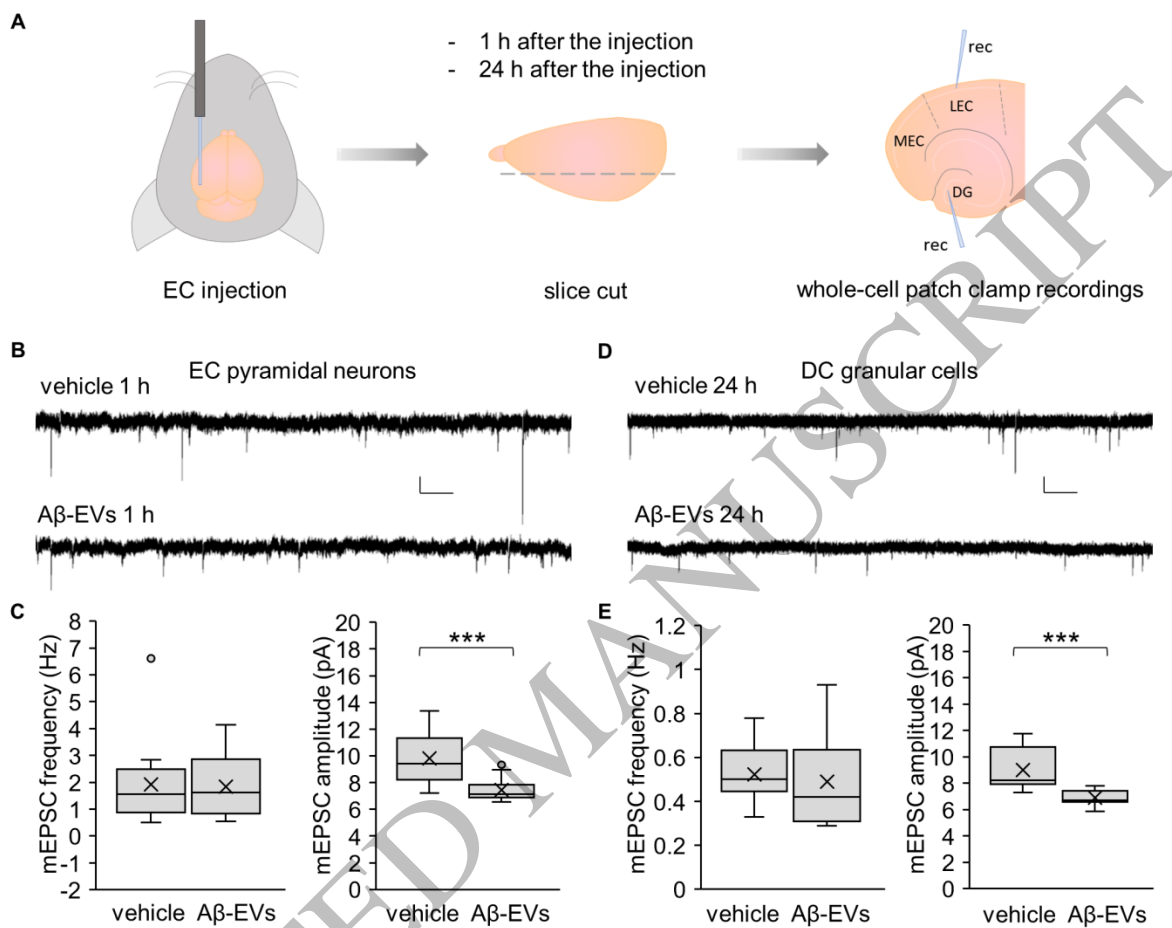


Fig. 5

Figure 5
190x160 mm (5.0 x DPI)

2

3

4

5

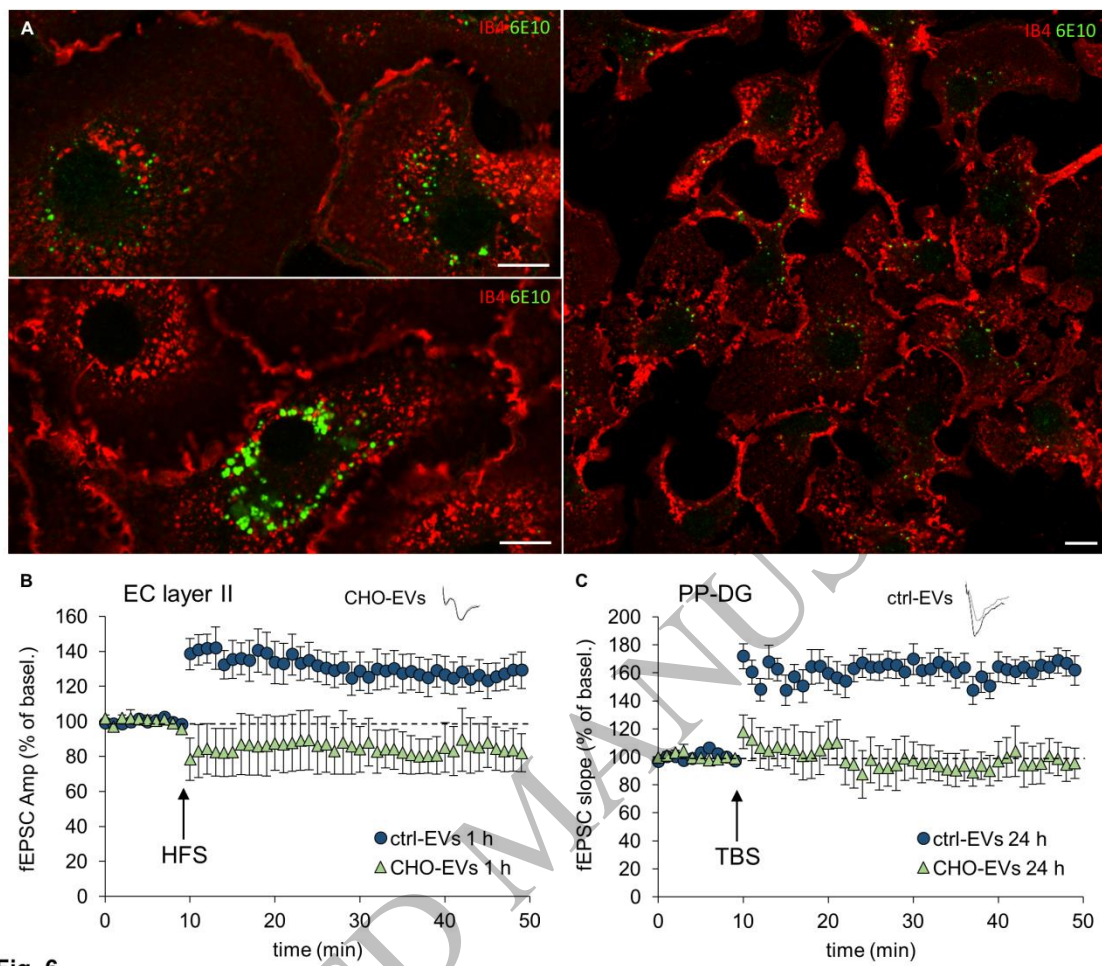


Fig. 6

Figure 6
220x178 mm (5.0 x DPI)

1
2
3
4

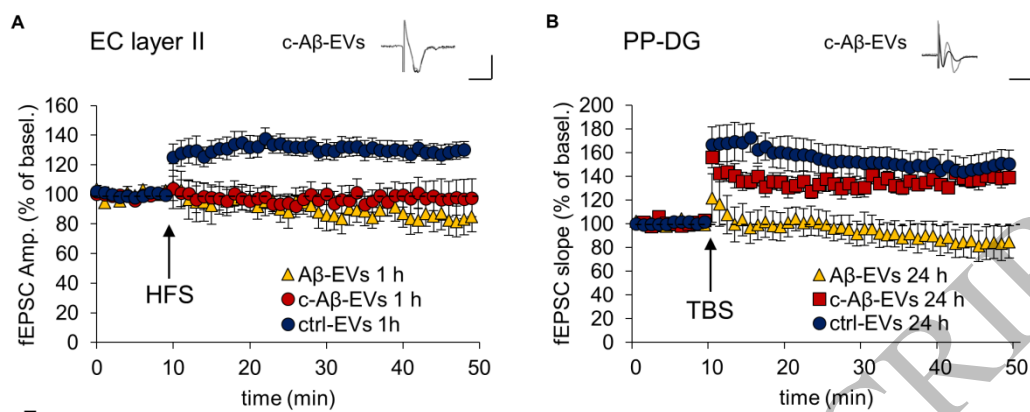


Fig. 7

Figure 7
210x90 mm (5.0 x DPI)

1
2
3
4

ACCEPTED MANUSCRIPT

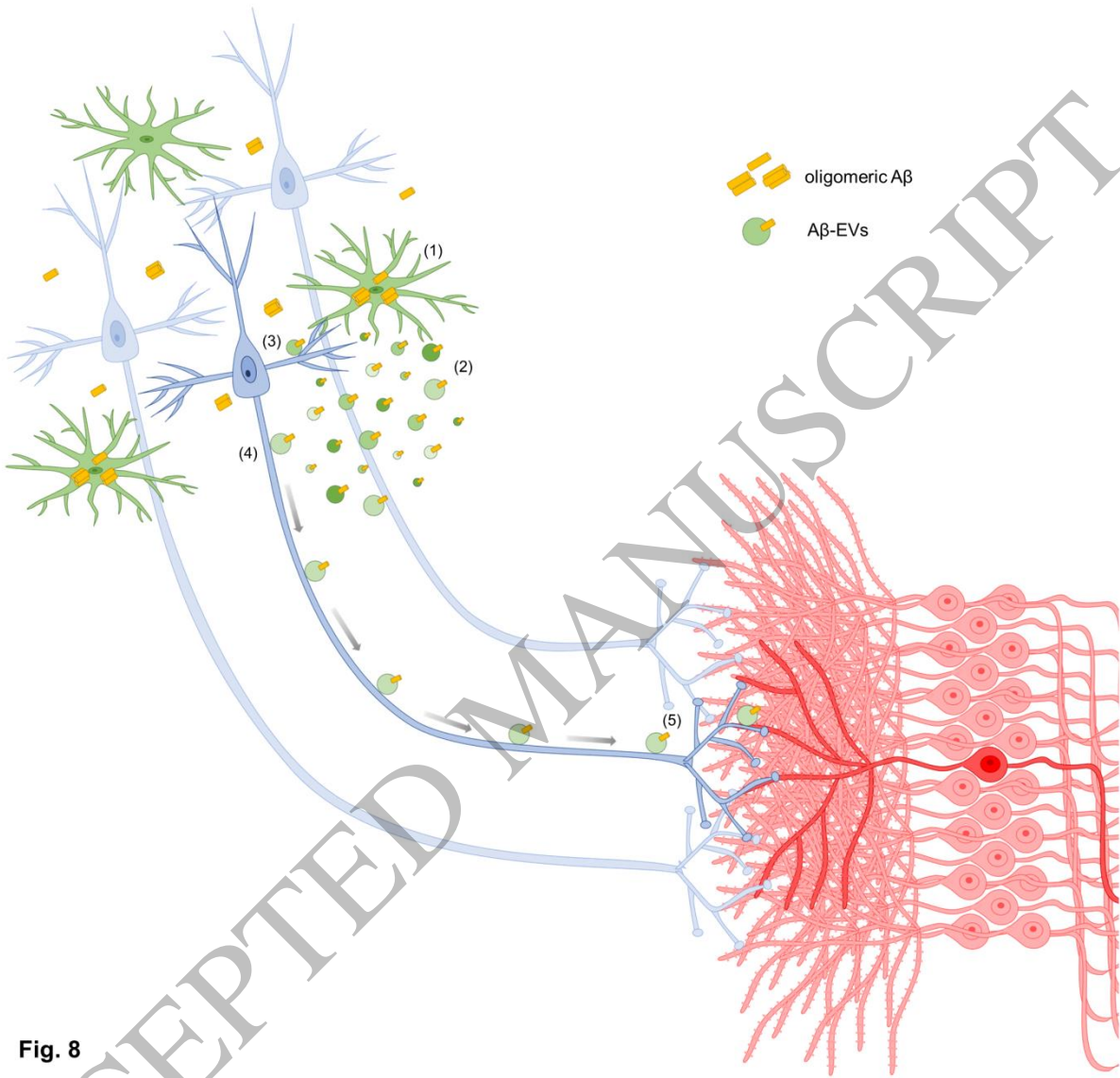


Fig. 8

Figure 8
210x200 mm (5.0 x DPI)

2
3
4

ACCEPTED MANUSCRIPT